



Modeling the climate impact of road transport, maritime shipping and aviation over the period 1860–2100 with an AOGCM

D. J. L. Olivie^{1,*}, D. Cariolle^{1,2}, H. Teyssède¹, D. Salas¹, A. Voltaire¹, H. Clark^{1,**}, D. Saint-Martin¹, M. Michou¹, F. Karcher¹, Y. Balkanski³, M. Gauss^{4,***}, O. Dessens^{5,****}, B. Koffi³, and R. Sausen⁶

¹GAME/CNRM, Météo-France, UMR1357, CNRS – Centre National de Recherches Météorologiques, Toulouse, France

²Sciences de l'Univers au CERFACS, CERFACS/CNRS, URA1875, Toulouse, France

³Laboratoire des Sciences du Climat et de l'Environnement, UMR8212, CEA-CNRS-UVSQ, Cedex, France

⁴Department of Geosciences, University of Oslo, Oslo, Norway

⁵Centre for Atmospheric Science, Department of Chemistry, University of Cambridge, Cambridge, UK

⁶Deutsches Zentrum für Luft- und Raumfahrt (DLR), Oberpfaffenhofen, Germany

* now at: Department of Geosciences, University of Oslo, Oslo, Norway

** now at: CNRS, Laboratoire d'Aérodynamique, UMR5560, Toulouse, France

*** now at: Norwegian Meteorological Institute, Oslo, Norway

**** now at: Energy Institute, University College London, London, UK

Correspondence to: D. J. L. Olivie (dirk.olivie@geo.uio.no)

Received: 10 May 2011 – Published in Atmos. Chem. Phys. Discuss.: 12 July 2011

Revised: 15 December 2011 – Accepted: 18 January 2012 – Published: 7 February 2012

Abstract. For the period 1860–2100 (SRES scenario A1B for 2000–2100), the impact of road transport, maritime shipping and aviation on climate is studied using an Atmosphere Ocean General Circulation Model (AOGCM). In addition to carbon dioxide (CO₂) emissions from these transport sectors, most of their non-CO₂ emissions are also taken into account, i.e. the forcing from ozone, methane, black carbon, organic carbon, sulfate, CFC-12 and HFC-134a from air conditioning systems in cars, and contrails. For the year 2000, the CO₂ emissions from all sectors together induce a global annual-mean surface air temperature increase of around 0.1 K. In 2100, the CO₂ emissions from road transport induce a global mean warming of 0.3 K, while shipping and aviation each contribute 0.1 K. For road transport, the non-CO₂ impact is largest between 2000 and 2050 (of the order of 0.1 K) becoming smaller at the end of the 21st century. The non-CO₂ impact from shipping is negative, reaching –0.1 K between 2050 and 2100, while for aviation it is positive and its estimate varies between 0 and 0.15 K in 2100. The largest changes in sea-level from thermal expansion in 2000 are 1.6 mm for the CO₂ emissions from road transport, and around –3 mm from the non-CO₂ effects of shipping. In 2100, sea-level rises by 18 mm due to the CO₂ emissions from road transport and by 4.6 mm due to shipping or avia-

tion CO₂ emissions. Non-CO₂ changes are of the order of 1 mm for road transport, –6.6 mm for shipping, and the estimate for aviation varies between –1.2 and 4.3 mm. When focusing on the geographical distribution, the non-CO₂ impact from road transport and shipping on the surface air temperature is only slightly stronger in northern than in southern mid-latitudes, while the impact from aviation can be a factor of 5 stronger in the northern than in the southern hemisphere. Further it is observed that most of the impacts are more pronounced at high latitudes, and that the non-CO₂ emissions from aviation strongly impact the NAO index. The impacts on the oceanic meridional overturning circulation and the Niño3.4 index are also quantified.

1 Introduction

In recent years, the evidence for anthropogenic impacts on climate (IPCC, 1996, 2001, 2007) has increased. Where observational studies have shown that the global mean surface air temperature has risen by around 0.8 K over the 20th century, modeling studies have demonstrated that this increase, in particular since the mid-20th century, can be attributed mainly to anthropogenic influences. Each activity which

alters the radiative properties of the atmosphere (by emission or formation of greenhouse gases (GHGs) and aerosols) or modifies the properties of the Earth's surface (a change in land-use can affect the local hydrological cycle or the albedo) may have an impact on climate. A wide range of anthropogenic activities such as industrial production processes, agriculture, transport, power generation, or domestic heating therefore possibly contributes to climate change.

It is important to quantify the contribution from individual sectors such as road transport, shipping, or aviation to climate change, because this allows more informed assessments of the potential effects of mitigation of emissions from these sectors, given the high growth rate of transport emissions in comparison to other anthropogenic sources. Over the last two decades, many studies have been performed which addressed this question – three recent reviews presented current assessments of the radiative forcing due to road (and rail) transport (Uherek et al., 2010), shipping (Eyring et al., 2010), and aviation (Lee et al., 2010) – see also Fuglestedt et al. (2008). From the transport sector, an important contribution to climate change is from carbon dioxide (CO₂) emissions, but the emissions of other species, including short lived ones, are also important. Several studies have assessed the impact of the emission of reactive gases (nitrogen oxides – NO_x, carbon monoxide – CO or volatile organic compounds – VOCs) on tropospheric ozone (O₃) and the hydroxyl radical (OH) from road transport (Granier and Brasseur, 2003; Niemeier et al., 2006; Matthes et al., 2007), shipping (Granier et al., 2006; Eyring et al., 2007) and aviation (Brasseur et al., 1996; Kentarchos and Roelofs, 2002; Gauss et al., 2006), or from all three sectors (Hoor et al., 2009; Koffi et al., 2010; Dahmann et al., 2011; Myhre et al., 2011). The present-day tropospheric O₃ changes lead to a radiative forcing between 10 and 30 mW m⁻² for the different transport sectors individually. These O₃ perturbations have a typical lifetime of a few weeks (Stevenson et al., 2004). Through the impact of NO_x emissions on the OH concentration, transport also affects the concentration of methane (CH₄). Generally, this is a reduction in the concentration of CH₄, and therefore a negative radiative forcing; the CH₄ reduction also leads to an associated reduction in O₃. Due to the long lifetime of CH₄, these perturbations have a lifetime in the order of 1 to 2 decades (Stevenson et al., 2004). For the current emissions from the transport sectors the net combined effect (from O₃ and CH₄) for road transport and aviation is a positive radiative forcing while it is negative for maritime shipping (Myhre et al., 2011).

The emissions from the transport sectors also lead to increased concentrations of aerosols such as black carbon (BC), organic carbon (OC) and sulfate. Aerosols have a direct impact through their scattering and absorption of radiation. This impact has been assessed for the three transport sectors in Balkanski et al. (2010) and in Eyring et al. (2007) for shipping only. Aerosols also have an indirect effect by changing the albedo (first indirect effect) and lifetime (sec-

ond indirect effect) of clouds as well as a semi-direct forcing due to BC – these forcings are much more uncertain (see Lee et al., 2010; Eyring et al., 2010; Uherek et al., 2010).

Several modeling and observational studies have tried to assess the global impact of contrails and aviation-induced cirrus (e.g. Bakan et al., 1994; Minnis et al., 2004; Marquart et al., 2003; Stordal et al., 2005; Burkhardt and K  rcher, 2009, 2011; K  rcher et al., 2010). Best estimates for the current radiative forcing due to contrail and aviation-induced cirrus impacts vary between 10 and 80 mW m⁻² (Lee et al., 2009). The most recent best estimates with the most detailed models of contrails and aviation-induced cirrus are at the lower end of this range, around 31 mW m⁻² (Burkhardt and K  rcher, 2011). Detailed process studies show an increased understanding of the formation and properties of contrails (Paugam et al., 2010).

In addition to detailed studies focussing on one or a few aspects of the impact of transport, some studies have tried to calculate its total radiative forcing (Fuglestedt et al., 2008; Penner et al., 1999). For aviation, multiple assessments have been made to assess its total impact (Brasseur et al., 1998; Penner et al., 1999; Sausen et al., 2005; Lee et al., 2009). As mentioned earlier, impacts on climate of all three modes of transport have recently been assessed (EU projects QUANTIFY and ATTICA) (Lee et al., 2010; Eyring et al., 2010; Uherek et al., 2010).

The impacts on climate in terms of changes in temperature and precipitation, are also of interest. Therefore, some studies use Atmosphere General Circulation Models (AGCMs) coupled to slab ocean models. Slab ocean models represent the ocean mixed layer but not the deep ocean, and they use prescribed local tendencies to represent large-scale ocean transport. These tendencies are assumed not to be affected by climate change, which might influence the quality of the climate predictions of this type of models. AGCMs coupled to a slab ocean model are used to study the climate change which would occur when the perturbation or anthropogenic influence is constant for a long period (e.g. Stuber et al., 2001, 2005; Joshi et al., 2003; Ponater et al., 2006), but are not able to describe so well the transient phase of climate change.

When the climate system is subject to a variable forcing, its thermal inertia will cause a delay in its response. Initially, there is a fast response of the atmosphere, the land surface and the ocean mixed layer with a characteristic time scale of 1 to 5 yr (e.g. Hasselmann et al., 1993; Boucher and Reddy, 2008; Oliv   and Stuber, 2010). This fast response contributes around 60–80 % to the total long term response. In addition, the deep ocean is responsible for a slow response (which contributes 20–40 %) with an estimated time scale in the order of 100 to 500 yr. For the study of the impact of the transport sectors, this inertia has been taken into account mainly in studies on aviation (Sausen and Schumann, 2000; Ponater et al., 2005, 2006; Lim et al., 2007; Lee et al., 2009). Also slightly more complicated Simple Climate Models (SCMs) which contain a simple representation

of ocean and sea-ice thermodynamics (Harvey et al., 1997; Skeie et al., 2009), have been used. They all simulate reasonably well the transient phase of climate change (Meinshausen et al., 2011a,b), but do not give information on the geographical distribution or seasonal variation of impacts.

A more complete but computationally more expensive approach is to use an Atmosphere Ocean General Circulation Model (AOGCM) which contains a detailed description of the atmosphere, ocean and sea-ice. Within the perspective of climate change, oceans play an important role in redistributing heat, in mitigating atmospheric heating in the transient phase due to their large thermal inertia, and in the radiative balance due to the possible presence of sea-ice at high latitudes (impact on albedo). Over the last decade, AOGCMs have been used frequently to model the total climate impact from anthropogenic forcing (IPCC, 2001). These models are currently able to reproduce the temperature change observed in the 20th century, and confidence exists in the quality of their projections of future climate change (IPCC, 2007, Chap. 8). This confidence is stronger at continental than regional scales, and higher for variables as temperature than for precipitation. However, although the AOGCMs are the most advanced tools, there remain important uncertainties in the representation of some processes, for example those defining the strength of cloud-climate feedbacks (IPCC, 2007). In addition, AOGCMs, when used to make global climate studies over multiple decennia or centuries, cannot be expected to describe all physico-chemical processes in the atmosphere in great detail, e.g. emissions, formation and transformation of aerosols and chemical species, and possible removal mechanisms. Therefore, distributions of long-lived GHGs are often assumed to be homogeneously distributed in the atmosphere (CO_2 , CH_4 , nitrous oxide – N_2O , and chlorofluorocarbons – CFCs), but their global concentration might evolve with time (according to a prescribed scenario). For aerosols and O_3 (or its precursors) which, due to their shorter lifetimes, are inhomogeneously distributed in the atmosphere, three-dimensional (3-D) prescribed climatologies are often used based on calculations from more detailed models. Here we present one of the first studies where an AOGCM is used to assess the impact of the transport sectors on climate. Using an AOGCM allows the study of geographical distributions of changes in surface air temperature, precipitation and cloud cover, and to quantify impacts on typical ocean parameters such as ocean 3-D temperature, sea-level rise, and the meridional overturning circulation (MOC). We study the period 1860–2100 and perform full 240-yr long integrations. We focus on the impact of road transport, maritime shipping and aviation, and distinguish between the impact from CO_2 emissions and the impact from all other emissions (which we call, collectively, non- CO_2).

In Sect. 2 we describe the AOGCM which is used, the emissions from the transport sectors that are taken into account, and the simulations which are performed. In Sect. 3 we analyze the impacts of the transport sectors on the atmo-

sphere, and in Sect. 4 their impacts on the ocean. In Sect. 5 we present our conclusions.

2 Description of the model, forcings and experiments

2.1 The CNRM-CM3.3 AOGCM

The Centre National de Recherches Météorologiques (CNRM) Coupled Model version 3.3 (CNRM-CM3.3) (Johns et al., 2011) consists of the atmosphere component ARPEGE-Climat4.6, the ocean component OPA8.0 and the sea-ice component GELATO2. CNRM-CM3.3 is an updated but very similar version of the CNRM-CM3.1 coupled model used for simulations described in Salas-Mélia et al. (2005), IPCC (2007) and Olivé and Stuber (2010).

The atmosphere component ARPEGE-Climat4.6 is a spectral model with a T42 horizontal resolution (equivalent to about $2.8^\circ \times 2.8^\circ$) and 31 hybrid sigma levels (model top at 10 hPa). Turbulent vertical fluxes and dry convection are described by Ricard and Royer (1993), and deep convection (Bougeault, 1985) is modeled using a mass-flux scheme with Kuo-type closure. The cloud microphysics is also described in Ricard and Royer (1993), and the model does not take into account ice supersaturation. The model uses the FMR15 radiation scheme (Morcrette, 1990, 1991), which considers two shortwave and six longwave spectral bands. The model takes into account the radiative impact of water vapour (H_2O), of the well-mixed GHGs CO_2 , CH_4 , N_2O , CFC-11, CFC-12, and of the O_3 and aerosol distributions, as well as clouds. Six types of aerosols (prescribed as monthly mean 3-D climatologies) are considered: continental (including BC and OC), marine, desert, volcanic, stratospheric, and sulfate aerosols. The model takes into account their direct effect, and the indirect effect of sulfate aerosols based on a parametrisation of Boucher and Rodhe (1994) and Boucher and Lohmann (1995) with a calibration from POLDER satellite data (Quaas and Boucher, 2005). The O_3 distribution is determined by a parametrisation of its homogeneous and heterogeneous chemistry (Cariolle and Déqué, 1986; Cariolle et al., 1990; Cariolle and Teyssèdre, 2007) (see further in Sect. 2.2.4). The model contains a description for river routing from Tokyo University (Oki and Sud, 1998; Oki et al., 1999). Changes in land use are introduced through a modification of the fractions of crop and pasture types in the land-surface classification, and the resulting surface properties have been computed with an updated version (ECOCLIMAP-2) of the ECOCLIMAP vegetation map (Champeaux et al., 2005). Both the ocean model OPA8.0 and the sea-ice model GELATO2 (Salas-Mélia, 2002) are grid point models and share the same mesh of 182×152 points. OPA8.0 has 31 levels, including 10 levels in the upper 100 m of the ocean.

The principal changes w.r.t. CNRM-CM3.1 are a revision of the atmosphere-ocean coupling through OASIS2.2

to achieve a better conservation of the energy fluxes during interpolations between the atmosphere and the ocean grids. Moreover, in the ocean and sea-ice models minor corrections have been implemented to improve energy conservation. These improvements have led to reduced drift in the ocean temperature fields and in surface air temperature. Finally, the atmospheric component of the model was updated from version 3 to 4.6.

The model (version CNRM-CM3.1 and CNRM-CM3.3) has been used to simulate both past and future climate change (Salas-M  lia et al., 2005; IPCC, 2007; Johns et al., 2011). In the historical simulation of the period 1860–2000 with CNRM-CM3.3, the heating (global mean surface air temperature) over the 1901–2000 period was 0.7 K, being slightly smaller than the observed trend over the 20th century (0.8 K, Brohan et al., 2006). Sea-ice distributions were reasonably well modeled (Salas-M  lia et al., 2005), and the deep convection sites simulated by OPA8.0 within CNRM-CM3.1 were found to be realistic (Gu  mas and Salas-M  lia, 2008).

2.2 Forcing agents

To model the climate change over the period 1860–2100, CNRM-CM3.3 takes into account changes in well-mixed GHGs, aerosols, total inorganic chlorine, and surface properties. Changes in the total solar irradiance and aerosols resulting from volcanic eruptions are not taken into account. For the period 2000–2100 we consider the SRES scenario A1B (Nakicenovic et al., 2000). The A1B scenario is based on the assumptions, for the 21st century, of rapid economic growth, further population increase until 2050 and a decline thereafter, global adoption of efficient technologies, and a balanced reliance on fossil- and non-fossil-fuel energy sources. In comparison to other SRES scenarios, this scenario results in a middle-of-the road increase in anthropogenic forcing. As the original SRES scenarios are not disaggregated enough, this general storyline was translated into specific emission scenarios for each transport sector individually (cf. Eyring et al., 2010; Lee et al., 2010; Uherek et al., 2010). The transport emission estimates for the 21st century are based on traffic demand estimates (which are assumed to be mainly driven by the gross domestic product (GDP) and population development), fuel efficiency estimates, and emission factor estimates (emission factors indicate how much $\text{NO}_x/\text{SO}_2/\text{BC}/\dots$ is emitted per unit fuel burnt). A distinction is made between different world regions, different vehicle, ship and aircraft types, different engine types and different fuel types. In scenario A1B, fuel consumption is assumed to grow for all three sectors, with some stabilization for road transport in the second half of the 21st century. For road transport (Uherek et al., 2010) it is assumed that emission standards will be taken over in the next decades on a global scale such that it will ultimately lead to a net decrease in NO_x emissions from 2030 on, despite the sustained increase in fuel consumption. For aviation (Lee et al., 2009, 2010; Owen et al., 2010), a sustained

fuel efficiency improvement is projected over the whole period 2020–2100 ($1\% \text{ yr}^{-1}$), and the emission factor for NO_x is assumed to decrease up to 2050 and remain constant thereafter. For shipping (Eyring et al., 2005, 2010; Eide et al., 2007), it is assumed that gas usage will increase rapidly and strongly, and legislation for reduced emission factors will be implemented at a moderate pace. One assumes that around 2050 maritime shipping will have fulfilled the full potential for emission reduction for the given engine types and fuel types (Eide et al., 2007). The estimated use of biofuels is moderate for shipping and low for aviation.

From the transport sectors, we take into account 6 different forcings. This includes for all sectors, the forcing from CO_2 , CH_4 , O_3 , and aerosols. In addition we take into account the emissions of CFC-12 and HFC-134a from road transport (from air conditioning systems in cars), and contrails and aviation-induced cirrus. The perturbations from CO_2 , CH_4 , CFC-12 and HFC-134a are assumed to be homogeneous perturbations (both horizontally and vertically), while the other perturbations have a geographical and vertical distribution. In Sect. 2.2.1 to 2.2.6, we describe the forcings in more detail.

Most of the emission data we use were developed during the QUANTIFY project, and can be found on <http://www.ip-quantify.eu/> (Borken et al., 2007). These data are spatially disaggregated with a $1^\circ \times 1^\circ$ horizontal resolution for each transport sector for the years 2000, 2025, 2050, 2100, and also include time series of decadal global emission estimates for the complete period 1860–2100. In this study we have taken the point of view that we limit the transport activity to the tailpipe emission plus the direct energy consumption to generate the fuel. An overview of the emissions by road transport, maritime shipping and aviation can be found in Tables 1, 2, and 3.

2.2.1 Carbon dioxide

Of all the CO_2 emitted in the atmosphere, about 10 % disappears from the atmosphere on relatively short time scales of around 1 to 2 yr. A large proportion of the emitted CO_2 stays much longer in the atmosphere as it is taken-up only slowly by oceans during the centuries following its emission. A significant fraction (between 20 and 30 %) of the CO_2 remains in the atmosphere on time scales longer than 1000 yr. CO_2 has thus a long residence time and is rather well mixed in the troposphere and the stratosphere (IPCC, 2007).

Figure 1a shows the evolution of the CO_2 concentration from 1860 until 2100 assuming the A1B emission scenario as developed in QUANTIFY for the transport sectors (<http://www.ip-quantify.eu/>) and the remaining CO_2 emissions from the respective marker scenario (Jiang et al., 2000). The CO_2 concentration has risen from 286 ppmv in 1860 up to 360 ppmv in 2000. One sees a further increase up to 700 ppmv in 2100. Figure 2 shows the distribution of the CO_2 emissions in 2000 from road transport, maritime

Table 1. Time series of road transport emissions (Borken et al., 2007; Uherek et al., 2010, <http://www.ip-quantify.eu/>). NO_x emissions are given as equivalent NO₂.

	NO _x Tg yr ⁻¹	CO Tg yr ⁻¹	CO ₂ Tg yr ⁻¹	BC Tg yr ⁻¹	OC Tg yr ⁻¹	SO ₂ Tg yr ⁻¹	CFC-12 Tg yr ⁻¹	HFC-134a Tg yr ⁻¹
1900	0.89	6.7	81	0.107	0.047	0.049	–	–
1910	1.20	8.9	109	0.143	0.063	0.066	–	–
1920	1.62	12.1	146	0.193	0.084	0.089	–	–
1930	2.18	16.3	197	0.260	0.114	0.119	–	–
1940	2.93	22.0	266	0.350	0.153	0.161	–	–
1950	5.16	38.6	467	0.616	0.269	0.283	–	–
1960	10.41	78.0	943	1.243	0.543	0.571	–	–
1970	19.00	138.9	1806	1.400	0.440	1.094	–	–
1980	26.30	158.5	2556	1.400	0.440	1.548	0.043	–
1990	32.78	192.0	3302	0.587	0.187	2.000	0.087	–
2000	29.17	109.2	4200	0.692	0.303	1.874	0.059	0.0568
2010	30.37	100.8	5555	0.664	0.289	0.422	–	0.136
2020	30.34	81.2	8230	0.350	0.149	0.153	–	0.152
2030	12.04	48.2	9860	0.070	0.034	0.065	–	0.106
2040	10.07	40.2	10768	0.057	0.027	0.036	–	0.060
2050	5.61	26.3	11376	0.028	0.014	0.039	–	0.014
2060	4.38	24.0	10850	0.022	0.011	0.038	–	–
2070	2.70	18.7	9758	0.014	0.007	0.034	–	–
2080	2.10	15.3	10331	0.010	0.005	0.036	–	–
2090	1.33	10.4	10425	0.006	0.003	0.036	–	–
2100	0.52	4.6	10450	0.001	0.001	0.036	–	–

Table 2. Time series of maritime shipping emissions (Endresen et al., 2003; Eyring et al., 2010, <http://www.ip-quantify.eu/>).

	NO _x Tg yr ⁻¹	CO ₂ Tg yr ⁻¹	BC Tg yr ⁻¹	OC Tg yr ⁻¹	SO ₂ Tg yr ⁻¹
1900	0.34	109	0.0062	0.0160	1.280
1910	0.52	167	0.0095	0.0244	1.957
1920	0.66	213	0.0121	0.0312	2.500
1930	0.77	247	0.0140	0.0362	2.800
1940	1.11	198	0.0112	0.0290	2.400
1950	2.12	261	0.0148	0.0383	3.800
1960	4.10	350	0.0199	0.0513	5.500
1970	11.10	480	0.0273	0.0703	7.600
1980	11.44	504	0.0286	0.0738	7.000
1990	12.13	534	0.0303	0.0783	6.900
2000	14.98	626	0.0355	0.1198	8.721
2010	17.43	845	0.0457	0.1543	8.553
2020	19.88	1065	0.0559	0.1888	8.384
2030	22.56	1393	0.0700	0.2364	8.520
2040	25.48	1832	0.0880	0.2972	8.960
2050	28.40	2271	0.1060	0.3580	9.400
2060	29.75	2811	0.1128	0.3808	7.705
2070	31.11	3350	0.1196	0.4036	6.009
2080	32.46	3890	0.1264	0.4264	4.314
2090	33.82	4429	0.1332	0.4492	2.618
2100	35.17	4969	0.1400	0.4720	0.923

Table 3. Time series of aviation emissions (Lee et al., 2010, <http://www.ip-quantify.eu/>).

	NO _x Tg yr ⁻¹	CO ₂ Tg yr ⁻¹	BC Tg yr ⁻¹	OC Tg yr ⁻¹	SO ₂ Tg yr ⁻¹
1940	0.09	28	0.0002	–	0.0036
1950	0.19	61	0.0005	–	0.0078
1960	0.41	132	0.0010	–	0.0168
1970	0.89	286	0.0021	–	0.0363
1980	1.34	407	0.0030	–	0.0516
1990	2.04	549	0.0041	–	0.0645
2000	2.80	677	0.0050	–	0.0873
2010	3.29	832	0.0062	–	0.1029
2020	4.00	1062	0.0078	–	0.1439
2030	5.12	1449	0.0105	–	0.2252
2040	6.54	1975	0.0140	–	0.3071
2050	7.50	2418	0.0169	–	0.3760
2060	9.51	3066	0.0214	–	0.3815
2070	11.28	3634	0.0254	–	0.3392
2080	12.91	4161	0.0290	–	0.2590
2090	14.42	4647	0.0324	–	0.1446
2100	15.72	5067	0.0354	–	0.0051

shipping and aviation. Because the CNRM-CM3.3 model does not represent the carbon cycle, it does not use CO₂ emissions as input data but needs prescribed CO₂ concentrations. These are taken from simulations with a SCM (Skeie et al., 2009) including a description of the carbon cycle (M. Lund, personal communication, 2009). These SCM simulations allow the derivation of the contributions from the different transport sectors to the total CO₂ concentration and it is this partitioning which is used in the CNRM-CM3.3 model. In our simulation, we use observed CO₂ concentrations until 2000 and the SCM modeled CO₂ concentrations from 2000 onwards. To avoid a discontinuity due to a small difference of around 3.5 ppmv between the observed and modeled CO₂ concentrations around 2000, we phase out this transition over the period 1990–2010.

Once the CO₂ contribution from each sector is known, it is possible to estimate the corresponding radiative forcing ΔF from CO₂ using the simple formula in IPCC (2001, Table 6.1),

$$\Delta F = 5.35 \text{ W m}^{-2} \times \log \frac{r_{\text{CO}_2}}{r_{\text{CO}_2}^0}, \quad (1)$$

where $r_{\text{CO}_2}^0$ and r_{CO_2} refer to the reference and perturbed CO₂ mixing ratios respectively. (Note that the radiative forcing in the AOGCM simulations are computed using the model's radiation scheme, rather than this simple formula.)

Figure 1c shows the radiative forcing from CO₂ by the different transport sectors. It is clear that road transport has the largest contribution. The evolution of the radiative forcing from shipping and aviation are very similar (this is specific for the A1B scenario), although the significant contribution from shipping starts somewhat earlier (around 1900) than the contribution from aviation (around 1940). The radiative forcing estimates compare reasonably well with the values in Fuglestad et al. (2008) for the year 2000 who obtained 150 mW m⁻² for road transport and 35 and 21 mW m⁻² for shipping and aviation, respectively.

2.2.2 CFC-12 and HFC-134a

Air conditioning systems in cars currently contain CFC-12 and HFC-134a, and these GHGs can end up in the atmosphere due to leakage or at the end of the car's lifetime (Clodic et al., 2005). Their radiative impact can be as large as 20 mW m⁻² and it is therefore taken into account here (G. R  del, personal communication, 2009). CFC-12 and HFC-134a are also used in cooling and freezing systems for the transport of goods, but we do not take this into account. Figure 1e shows the radiative forcing by these two gases. For the radiative efficiency we use 0.32 and 0.16 W m⁻²ppb⁻¹ for CFC-12 and HFC-134a, respectively (IPCC, 2001, Table 6.7). Due to the relatively long lifetimes (100 and 14 yr for CFC-12 and HFC-134a, respectively), their effect goes on well beyond the emission periods (CFC-12 emissions from

cars span the 1970 to 2010 period and peak around 1990–1995, HFC-134a emissions span the 1993–2053 period and peak around 2015). We do not take into account the impact from these extra CFC-12 and HFC-134a emissions on stratospheric O₃ destruction. Uherek et al. (2010) estimated that this impact is smaller than –10 mW m⁻² in the period 1980–2000.

2.2.3 Methane

The evolution of the CH₄ mixing ratio for the SRES scenario A1B is shown in Fig. 1b: the large increase during the 20th century continues in the first half of the 21st century followed by a decrease. The transport sectors also have an impact on the CH₄ concentration, not by direct CH₄ emissions which are assumed small for the transport sectors, but by an enhanced destruction of CH₄ by increased OH concentrations related to NO_x emissions. This impact is often expressed as a reduction of the CH₄ lifetime (Prather, 1994). For the transport volumes of the year 2000, Hoor et al. (2009) calculated for each sector, the impact on the OH distribution. As the reaction with OH is the principal sink of CH₄, one can use these results to obtain the reduction in CH₄ lifetime by each transport sector. For the year 2000, they found reductions of the CH₄ lifetime of 1.61, 4.12 and 1.04 % for road transport, shipping and aviation, respectively (including the feedback factor to include the long term equilibration to the new steady-state, Fuglestad et al., 1999). Their results were obtained using 6 different chemistry transport models (CTMs), driven by meteorological analyses for the year 2003 from the European Centre for Medium-range Weather Forecasts (ECMWF).

We use OH perturbation fields very similar to those of Hoor et al. (2009), derived from simulations by 3 CTMs (p-TOMCAT, LMDZ-INCA and Oslo-CTM2) which used updated emissions for road transport and aviation (Koffi et al., 2010; Hodnebrog et al., 2011). In addition to transport volumes for 2000, the OH impact was also calculated for the assumed transport volumes in 2025 and 2050, with the same 2003 meteorological analyses.

Using the average of the OH distributions obtained with these 3 CTMs, CH₄ lifetimes and lifetime changes for the years 2000, 2025 and 2050 are calculated. For intermediate years over the period 1860–2100 where no CTM results are available, we linearly interpolate or extrapolate the CH₄ lifetime, scaling the CH₄ lifetime change caused by a specific sector with the total global NO_x emission from that sector. The time series of the total NO_x emission for the different sectors are shown in Fig. 1g. Using these CH₄ lifetimes τ and lifetime changes $\Delta\tau$ and assuming that the transport sector does not contribute to the CH₄ emissions, one can calculate the impact of the reduced CH₄ lifetime on the CH₄ concentration from the differential equation

$$\frac{d\Delta r_{\text{CH}_4}}{dt} = -\frac{\Delta r_{\text{CH}_4}}{\tau} + \frac{r_{\text{CH}_4}^0}{\tau} \frac{\Delta\tau}{\tau}, \quad (2)$$

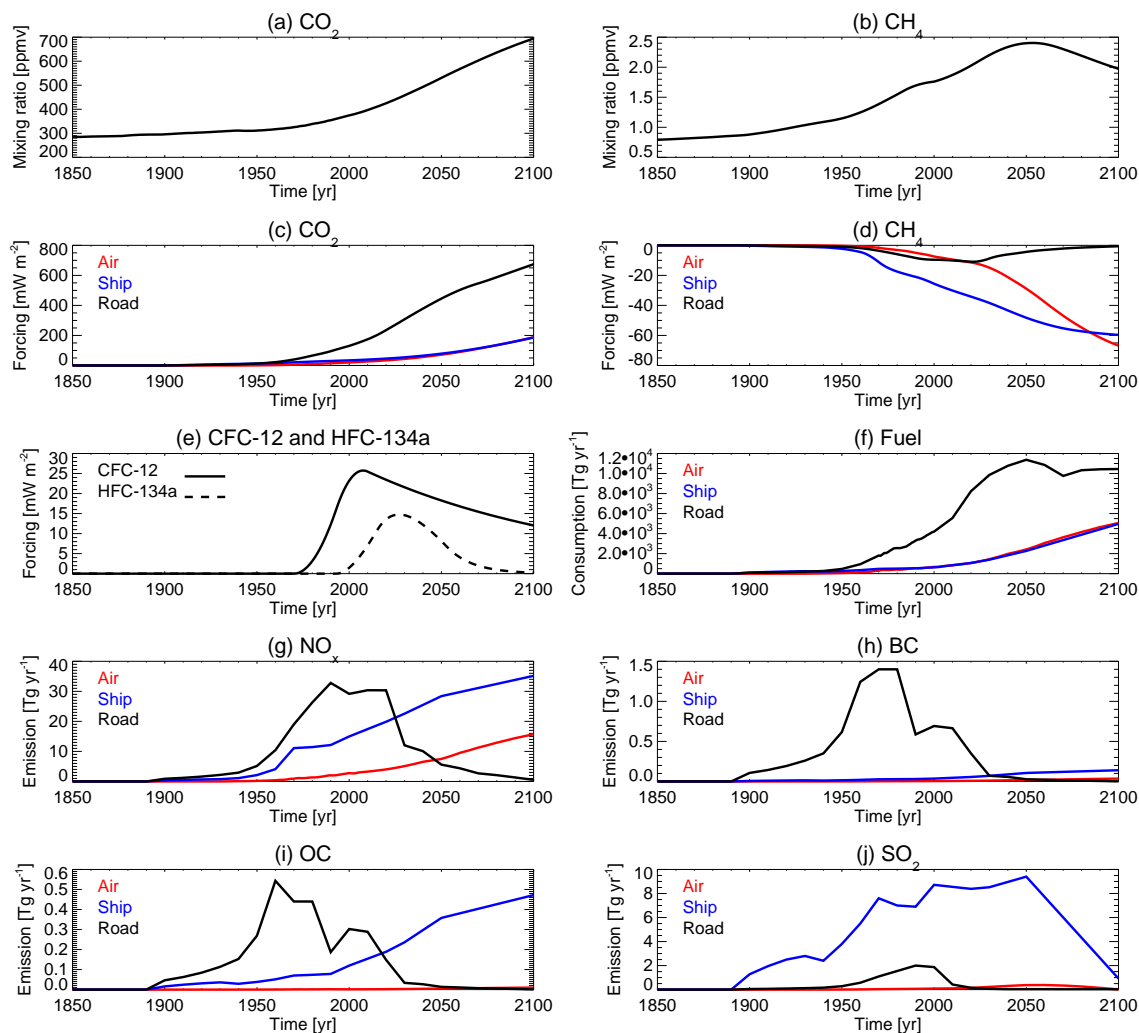


Fig. 1. Time series of the forcings taken into account in the model integrations over the period 1860–2100. The first row shows the evolution of (a) CO₂ and (b) CH₄ mixing ratios in the reference simulation. Row 2 until 5 show forcings and emissions from the transport sectors: (c) radiative forcing from CO₂, (d) radiative forcing from CH₄, (e) radiative forcing from CFC-12 and HFC-134a from road transport, (f) global annual fuel consumption, and emissions from (g) NO_x, (h) BC, (i) OC and (j) SO₂.

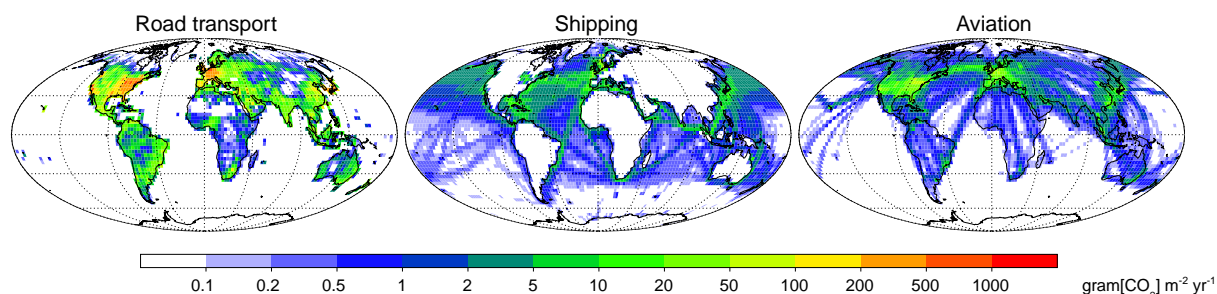


Fig. 2. Global maps of the annual CO₂ emission estimates (in gram[CO₂] m⁻² yr⁻¹) for the year 2000 from road transport (left), maritime shipping (middle) and aviation (right). For more details, see Borken et al. (2007), Endresen et al. (2003), Lee et al. (2010), and <http://www.ip-quantify.eu/>.

where one takes the background evolution of methane $r_{\text{CH}_4}^0$ from IPCC (2001, Appendix II). In this approach we disregard the stratospheric and soil sinks for CH₄ with lifetimes of 120 and 160 yr, respectively (IPCC, 2001). Also, one must be aware that the reference CH₄ lifetime is based on the mentioned CTM simulations and does not necessarily agree with the lifetime used in IPCC (2001), and therefore might hamper a coherent reconstruction. Figure 1d shows the reduction of radiative forcing due to CH₄ perturbations for the different sectors, calculated using IPCC (2001, Table 6.2). Shipping has the strongest impact on the CH₄ lifetime (Hoor et al., 2009) and thus on its concentration and radiative forcing. Both shipping and aviation show an increasing impact of CH₄ in the 21st century due to increasing NO_x emissions. At the end of the 21st century the impact from aviation on CH₄ even equals the shipping impact. We do not take into account the impact from CH₄-induced O₃ changes, which might add an extra 42 % negative radiative forcing (Hoor et al., 2009).

2.2.4 Ozone

CNRM-CM3.3 contains a simplified O₃ chemistry description which was specifically developed to simulate stratospheric O₃ in AGCMs (Cariolle and D  qu  , 1986; Cariolle et al., 1990; Cariolle and Teyss  dre, 2007). To be able to account for the tropospheric and lower stratospheric O₃ changes induced by the transport sectors, we additionally use information from the CTM simulations mentioned earlier. From these simulations, the impacts of transport on O₃, NO_x, CO, and many other atmospheric components (e.g. OH, see Sect. 2.2.3) were obtained for the years 2000, 2025 and 2050.

To take into account the O₃ impact from transport, we use two different methods. In a first approach (dynamical O₃ approach), we use an extended version of the linear O₃ scheme. As the tropospheric O₃ production is strongly dependent on the NO_x and CO mixing ratio, the linear O₃ parametrization of the AOGCM (Cariolle and Teyss  dre, 2007) has been extended to take into account the impact of NO_x, CO and H₂O perturbations on the net O₃ production. The net O₃ production P is approximated by

$$P = c_0 + c_1(T - c_2) + c_3(\Sigma_{\text{O}_3} - c_4) + c_5(r_{\text{O}_3} - c_6) + c_7 r_{\text{Cl}_y}^2 \theta(T_c - T) \theta(\phi_c - \phi) + c_8(r_{\text{NO}_x} - c_9) + c_{10}(r_{\text{CO}} - c_{11}) + c_{12}(r_{\text{H}_2\text{O}} - c_{13}), \quad (3)$$

with T the temperature, Σ_{O_3} the local overhead total O₃ column, ϕ the solar zenith angle, θ the unit step function, and r_{O_3} , r_{NO_x} , r_{CO} , and $r_{\text{H}_2\text{O}}$ the mixing ratios of the indexed species. The coefficients c_0, c_1, \dots, c_{13} are zonal monthly climatologies derived with the 2-D stratospheric chemistry transport model MOBIDIC (Cariolle and Teyss  dre, 2007). Coefficient c_7 (≤ 0) represents stratospheric heterogeneous destruction with r_{Cl_y} the total inorganic chlorine mixing ratio. The factor $\theta(T_s - T) \theta(\phi_c - \phi)$ with θ the unit step function assures that the heterogeneous destruction is only ac-

tive below a threshold temperature $T_s = 195$ K and for solar zenith angles smaller than $\phi_c = 90^\circ$. The coefficients c_8, \dots, c_{13} describe the linearized impact of NO_x, CO and H₂O on the net O₃ production. In this setup the NO_x, CO and H₂O fields can be seen as external forcings, in the same way AOGCMs often use prescribed aerosol climatologies. The zonal-mean distributions of the NO_x perturbations can be seen in Fig. 3a, representative for June-July-August (JJA) around the year 2000. In the current study, we do not use the dependency on the H₂O concentration, and for CO we only use it for the impact from road transport. To obtain the net O₃ production for other years than 2000, 2025 or 2050, we scale the NO_x and CO perturbation fields with the total global NO_x and CO emissions (<http://www.ip-quantify.eu/>).

In a second approach (fixed O₃ approach), we use the 3-D O₃ perturbations originating from the CTMs directly in the AOGCM. These perturbations can be seen in Fig. 3b and are added to the background O₃ described by Eq. (3), but now with $c_8 = c_9 = c_{10} = c_{11} = c_{12} = c_{13} = 0$. To obtain perturbation fields for years other than 2000, 2025 or 2050, we scale the O₃ perturbations with the NO_x emissions, assuming that NO_x is the predominant factor for tropospheric and lower stratospheric O₃ perturbations.

2.2.5 Contrails and aviation-induced cirrus

When describing the clouds generated by aircraft, one usually distinguishes between linear contrails (condensation trails) and aviation-induced cirrus. Contrails are line-shaped cirrus clouds produced in the wake of an aircraft when hot and moist air from the exhaust mixes with ambient air that is below a critical temperature (Schumann, 1996). Observational studies have been performed using satellite images to estimate the presence of contrails (Mannstein et al., 1998). Different modeling studies have estimated the cloud cover and radiative forcing associated with linear contrails (Marquart et al., 2003; R  del and Shine, 2008; Rap et al., 2010), where the contrail coverage has been parameterized relying on observed values for the contrail formation frequency (Bakan et al., 1994). Lee et al. (2009) estimated the impact in 2005 of 12 mW m⁻². When linear contrails persist, they can give rise to aviation-induced cirrus which due to the loss of the linear shape become indistinguishable from natural cirrus clouds. Therefore aviation-induced cirrus is much more difficult to estimate. Stordal et al. (2005) have used 16 yr of observational cloud data (1984–1999) to estimate the increase or decrease in the presence of cirrus, and derived a radiative forcing of 30 mW m⁻² that includes both linear contrails and aviation-induced cirrus. Recently, modeling studies have been performed which model the evolution and aging of contrails: Burkhardt and K  rcher (2009, 2011) derived a radiative forcing of 31 mW m⁻².

We use in CNRM-CM3.3 a simple description of the major forcing from linear contrails and aviation-induced cirrus. To model the possible presence of linear contrails and

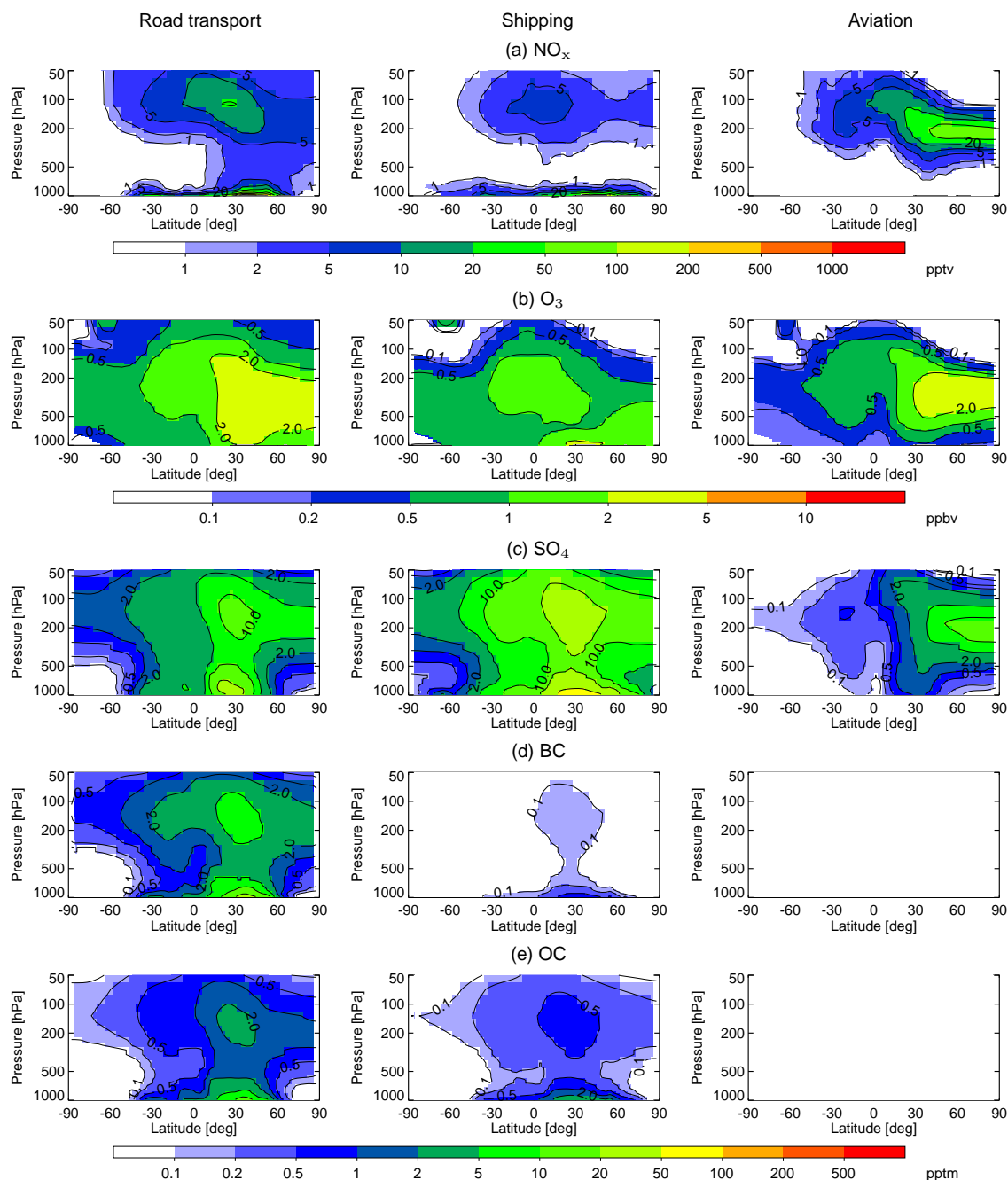


Fig. 3. Contribution by road transport (left), shipping (middle) and aviation (right) to the distribution of (a) NO_x (pptv), (b) O_3 (ppbv), (c) sulfate (ppt), (d) BC (ppt), and (e) OC (ppt) in JJA 2000. These contributions are obtained by off-line CTM simulations: O_3 and NO_x are averages over the p-Tomcat, LMDZ-INCA and Oslo-CTM2 models, while the aerosol fields are those of the LMDZ-AER model.

aviation-induced cirrus in the regions with dense air traffic, we use a “recent exhaust” distribution obtained with a CTM (Teyssèdre et al., 2007). We model the distribution of this tracer for the years 2000, 2025, 2050 and 2100, taking as its source the fuel consumption, assuming a lifetime varying with height (i.e. 15 h at 250 hPa and 2 h at 850 hPa), and integrating the large scale transport with ECMWF meteoro-

logical analyses for 2003. For aviation, monthly 3-D fuel consumption data are available for the years 2000, 2025, 2050, and 2100 (<http://www.ip-quantify.eu/>). The monthly mean distribution of the “recent exhaust” tracer is used in CNRM-CM3.3 to indicate air masses affected by recent air traffic. We assume that high concentrations of this tracer can induce a cirrus cloud if the temperature is below -40°C

Table 4. Time series of mixing ratios of GHGs and total inorganic chlorine as used in the reference simulation.

	CO ₂ ppmv	CH ₄ ppbv	N ₂ O ppbv	CFC-11 pptv	CFC-12 pptv	Chlorine pptv
1850	285	792	276	12.5	0.0	484
1860	286	806	277	12.5	0.0	484
1870	288	821	277	12.5	0.0	484
1880	291	837	278	12.5	0.0	484
1890	294	857	279	12.5	0.0	484
1900	296	879	280	12.5	0.0	484
1910	300	924	281	12.5	0.0	485
1920	303	978	283	13.1	0.0	490
1930	308	1036	286	14.6	0.0	503
1940	311	1089	288	19.8	0.3	547
1950	311	1148	290	32.8	6.8	661
1960	317	1248	293	50.6	32.6	805
1970	326	1386	296	134.0	123.3	1321
1980	339	1547	302	329.8	307.7	2424
1990	354	1694	308	563.3	485.2	3471
2000	375	1760	316	653.5	535.0	3453
2010	397	1871	324	778.3	527.3	3336
2020	425	2026	331	785.8	485.7	3009
2030	458	2202	338	769.1	440.8	2622
2040	493	2337	344	834.0	399.6	2321
2050	531	2400	350	948.8	362.3	2061
2060	568	2386	356	1083.3	328.5	1850
2070	603	2301	360	1199.1	297.8	1683
2080	636	2191	365	1264.6	270.0	1546
2090	667	2078	368	1303.4	244.8	1431
2100	694	1974	372	1315.9	222.0	1331

and if the relative humidity is above 80 % (R  del and Shine, 2008). We impose this 80 % limit as the current version of the atmospheric model does not consider ice supersaturation. The relationship between the recent exhaust tracer and the presence of linear contrails or aviation-induced cirrus is calibrated to have a top of the atmosphere (TOA) radiative forcing of 0.024 W m⁻² for the year 2000 (slightly lower than the 31 mW m⁻² in Burkhardt and K  rcher, 2011). This value of 0.024 W m⁻² is based on the assumptions that the impact from linear contrails alone is 0.006 W m⁻² in the year 2000 (R  del and Shine, 2008) and that the impact of aviation-induced cirrus is 3 times larger than from linear contrails (Fuglestad et al., 2010). Using these distributions in CNRM-CM3.3, we find TOA net radiative forcings in 1980, 2000, 2025, 2050 and 2100 of 14.9, 24.1, 44.2, 101 and 211 mW m⁻², respectively. In tests where we impose a global uniform contrail coverage of 0.01, 0.1 and 1 with a contrail optical depth of 0.3, we find net TOA radiative forcings of 0.16, 1.63 and 15.1 W m⁻². This value of 0.16 W m⁻² corresponds well with the values mentioned in Myhre et al. (2009) which is a comparative study among different line-by-line radiative transfer codes and codes used in AGCMs, including the one used in CNRM-CM3.3. For an experiment with a 0.01 global contrail cover at 0.3 opti-

cal depth, where the grey body emissivity formulation had been replaced by a two-stream approximation in order to accommodate the prescribed optical properties of the contrail, a value of 0.19 W m⁻² was reported for CNRM-CM3.3, close to the best estimate of 0.163 W m⁻². Myhre et al. (2009) further mention that for this experiment they found a strong similarity in the spatial pattern of the radiative forcing among the models, with rather low values at high latitudes. For years other than 2000, 2025, 2050 and 2100, we interpolate the 3-D recent exhaust tracer distributions scaling them with the global annual fuel consumption by aviation, which can be found in Fig. 1f.

2.2.6 Aerosols

The CNRM-CM3.3 model accounts for both direct and indirect effects of aerosols. The indirect effect is however limited to the sulfate component, which leads to an underestimation of the total indirect effect. As the transport sectors are a source of aerosols in the atmosphere, we take into account the BC, OC and sulfate aerosols from the different transport sectors, and use monthly mean 3-D distributions which are available from simulations with the INCA-AER model (Balkanski et al., 2010), using the emissions from <http://www.ip-quantify.eu/>. Figure 3c–e shows the zonal mean distribution of the perturbation in BC, OC and sulfate aerosols induced by the different transport sectors in JJA 2000. We use these 3-D aerosol distributions in the AOGCM in addition to the standard aerosol distributions in the model. For the year 2000, we find optical depths at 550 nm similar to those of Balkanski et al. (2010, Table 2). However, changes in net incoming radiation at the TOA are quite different. BC induces changes at the TOA of 1.15, 0.027 and 0.00014 mW m⁻² for road transport, shipping and aviation respectively, which is at least a factor 40 lower than mentioned in Balkanski et al. (2010). This will mainly have an impact on the road transport sector (see Fig. 1h). With correct forcings one would probably see a slight increase in the warming from the road sector, although this would depend on the poorly understood semi-direct effect of BC on clouds. For OC we find equally small values. For sulfate we find changes at the TOA of -32.2, -95 and -4.5 mW m⁻² for road transport, shipping and aviation, respectively. This is considerably more than the values in Balkanski et al. (2010), which only included the direct aerosol effect. As we also include the first indirect aerosol effect, part of the differences can be attributed to that.

To obtain the aerosol distribution for years other than 2000, we scale the 3-D distribution with the annual global BC, OC, and SO₂ emissions (see Fig. 1h–j). Road transport is the main contributor to BC and OC emissions, while the SO₂ emissions are strongest for shipping however showing a large reduction at the end of the 21st century. The SO₂ emissions from aviation, that peak around 2050, are much lower than from shipping.

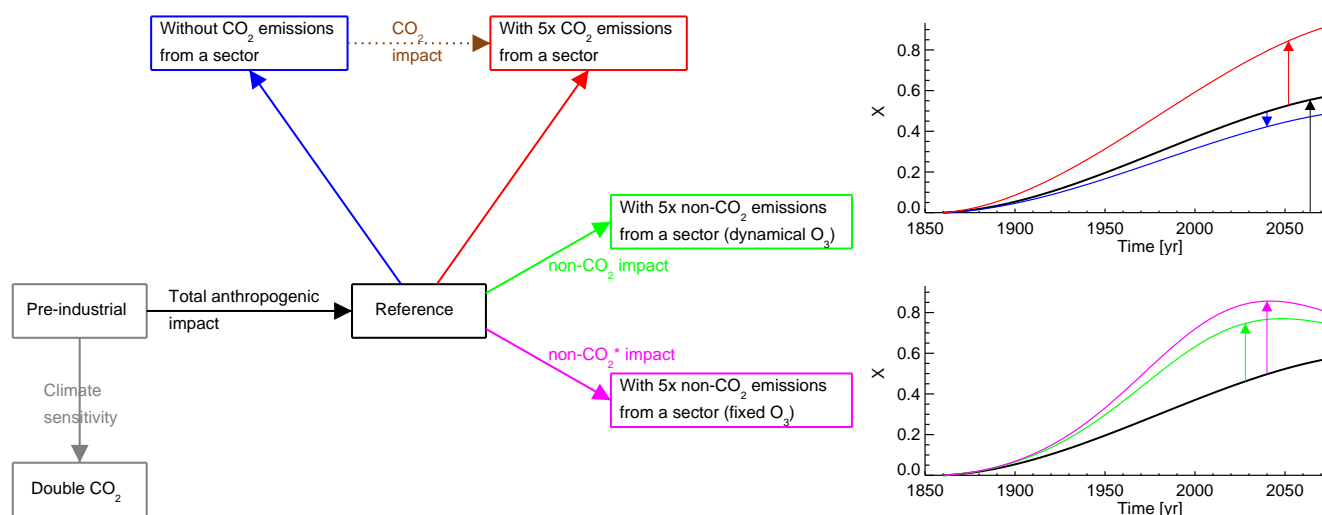


Fig. 4. Schematic representation of the different simulations and impacts (a general impact is represented by X in the ordinate). The black curve (box) denotes the simulation which takes into account all the anthropogenic forcings. The other coloured curves (boxes) represent simulations where the CO₂ or non-CO₂ emissions of one of the transport sectors are modified. The blue curve (box) denotes a simulation without CO₂ emissions of one of the transport sectors, and the red curve (box) denotes a simulation with 5 times the CO₂ emissions of the same sector. The green curve (box) indicates a simulation with 5 times the non-CO₂ emissions from one transport sector, using the dynamical O₃ approach. The purple curve (box) indicates a simulation with the same emissions but using the fixed O₃ approach (see Sect. 2.2.4). A simulation with doubled CO₂ concentration (grey box) is used to derive the climate sensitivity.

2.3 Experiments

We perform several simulations with the CNRM-CM3.3 model over the period 1860–2100. A schematic picture of the different simulations can be found in Fig. 4. The reference simulation (see black curve and black box in Fig. 4) uses the standard forcings to model the evolution of the Earth’s climate over the period 1860–2100 (scenario A1B from 2000 onwards). The CO₂ and CH₄ evolutions used are shown in Fig. 1a–b, but also N₂O, CFC-11, CFC-12, the surface properties and the sulfate aerosol evolve with time. An overview of the time series of prescribed GHGs as used in the reference simulation can be found in Table 4. Comparing this simulation with a simulation under pre-industrial conditions (grey box in Fig. 4) allows the derivation of the “total anthropogenic impact”.

To study the impact of the different transport sectors, we perform a number of sensitivity simulations (also indicated in Fig. 4), making separate simulations to quantify the CO₂ and non-CO₂ impact. The non-CO₂ impact includes the effects from O₃, CH₄, CFC-12 and HFC-134a, aerosols, and contrails. To study the CO₂ impact, we do two types of simulations, represented in the upper right panel of Fig. 4: a first one without the CO₂ contribution from a certain sector (blue curve), and a second one with five times the CO₂ contribution from that sector (red curve). To study the non-CO₂ impact (see lower right panel in Fig. 4), we perform simulations where we add 5 times the non-CO₂ forcing from a certain sector w.r.t. the reference simulation. We perform simula-

tions using the dynamical O₃ approach (which we will call non-CO₂, green line or box in Fig. 4), and simulations using the fixed O₃ approach (which we call non-CO₂*, purple line or box in Fig. 4). Each simulation is repeated 3 times, using different initial conditions for the ocean, sea-ice and atmosphere, resulting in small ensembles of 3 members. The initial conditions for the members of the ensembles are taken from a pre-industrial simulation with a 10 yr time interval. Figure 5 indicates how the use of ensembles and amplification of the forcings reduces the overlap between the uncertainty interval of the reference experiment and a perturbation experiment: using more members in an ensemble reduces the size of the uncertainty interval, and amplifying the forcing increases the spacing between these intervals. Note that due to non-linearity, the best estimate based on an amplification of the forcing (red dot, Fig. 5) might be different from the actual impact (grey S1 dot).

As the emissions of the transport sectors are assumed negligible before 1890, our perturbation simulations do not show any impact before 1890. Because shipping and aviation have almost the same temporal evolution for their CO₂ contribution in scenario A1B (see Fig. 1c), we perform only one simulation that represents the CO₂ impact for both sectors. We also make a 100-yr long simulation where we double the CO₂ mixing ratio (grey box in Fig. 4) w.r.t. the pre-industrial value to estimate the climate sensitivity according to Gregory et al. (2004).

Finally, we want to mention that we do not consider certain forcings from the transport sectors such as the impact of BC

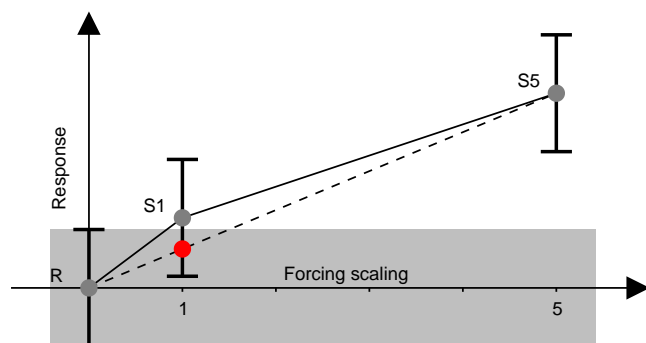


Fig. 5. Schematic representation of the impact of ensemble size and amplification of the forcing on the signal-to-noise ratio. The response (y-axis) is represented as a function of the size of the forcing (x-axis) in (R) a reference simulation, (S1) a simulation including once the forcing from a transport sector, and (S5) a simulation including 5 times the forcing from that transport sector. The black vertical bars indicate the uncertainty on the experiments best estimates. Increasing the ensemble size reduces these uncertainties. Note that due to non-linearity, the best estimate based on an amplification of the forcing (red dot) might be different from the actual impact (grey S1 dot).

on the formation of ice clouds (Penner et al., 2009; Liu et al., 2009), the impact of N_2O emissions (conversion of NO_x into N_2O in catalytic converters in cars), the impact of water vapour emissions from aircraft in the upper troposphere or lower stratosphere, the direct impact of CH_4 emissions, the impact of CH_4 changes on stratospheric water vapour, or the impact of CH_4 changes on O_3 . We also do not take into account the indirect impact of increased O_3 concentrations (from NO_x emissions) on the CO_2 uptake by vegetation (Sitch et al., 2007; Collins et al., 2010). Furthermore, in our approach resultant climate impacts do not feed back or affect the forcing mechanisms. E.g. OH, NO_x , and O_3 distributions for the year 2050 have been calculated using 2050 emissions but using year 2000 (or 2003) meteorology, such that impacts of possibly warmer and wetter conditions on the presence of these species are not taken into account. Expected impacts of changes in precipitation on aerosol distributions are not taken into account either. Several studies (Brasseur et al., 2006; Wu et al., 2008; Hedegaard et al., 2008; Koffi et al., 2010) investigated the impact of climate change on tropospheric chemistry and aerosols. Over the period 2000–2050, Wu et al. (2008) found that OH changes from climate change prevail on changes from emissions, while O_3 changes are mainly driven by emission changes (Brasseur et al., 2006; Wu et al., 2008; Koffi et al., 2010). Hedegaard et al. (2008) found both regions with increasing and decreasing wet deposition of aerosols, but none of these changes were significant in their simulations.

3 Atmosphere

In this section, we describe the impact of the 3 transport sectors on some key aspects of the atmosphere over the period 1860–2100: O_3 , TOA forcing, surface air temperature, atmospheric temperature profiles, precipitation, cloud cover, and the NAO index. We show the separate impact of the transport sectors and distinguish between the CO_2 and non- CO_2 impacts, and, as a reference, we also show the total anthropogenic impact. We show time averages over 4 different periods, i.e. 1980–1999, 2011–2030, 2046–2065 and 2080–2099, which also have been studied in IPCC (2007).

3.1 Ozone

We use two different methods to take into account the O_3 perturbations. In the first method (dynamical O_3 approach) we impose 3-D NO_x and CO perturbations which are used by the extended linear O_3 scheme to calculate the net O_3 production. The actual resulting O_3 mixing ratio might differ considerably from the prescribed O_3 perturbations of the second (fixed O_3) approach, where we impose 3-D O_3 perturbations directly. Figure 6a–d shows the impact from the transport sectors on the evolution of the O_3 mixing ratio at 850 and 250 hPa in the SH and NH. At 850 hPa, there is a reasonable agreement between the dynamical and fixed O_3 approaches. The correspondence is rather strong in the SH and for shipping in the NH, but the impacts from road transport and aviation in the NH differ by a factor of 2. In general, the dynamical approach leads to larger O_3 perturbations. For both approaches, we see stronger impacts in the NH than in the SH. Shipping has the smallest hemispheric difference, with an impact in 2100 of slightly more than 3 ppbv in the NH and slightly less than 2 ppbv in the SH. The impact of road transport is strongest between 1990 and 2020, and decreases rapidly after 2020. Finally one can see that at the end of the 21st century the impact of aviation and shipping are of similar magnitude. At 250 hPa, the differences between the dynamical and fixed O_3 approach become especially large for aviation. The impact at 250 hPa is generally dominated by aviation, whereas before 2020 the impact in the SH from road is dominant. The impact from aviation in the SH is almost a factor of 5 smaller than in the NH, a consequence of the much stronger emissions in the NH, the short tropospheric O_3 lifetime and the slow inter-hemispheric mixing.

Figure 6e–f shows the evolution of the total O_3 column in Dobson Units (DU), due to the total anthropogenic impact (left, absolute columns), and due to transport impacts (right, changes in O_3 columns). The O_3 column is around 315 DU in the first part of the 20th century, but at the end of the 21st century it reaches 325 DU. This increase is related to the impact of a colder stratosphere in a changing climate on O_3 concentrations. The Antarctic O_3 hole is manifest in the second half of the 20th and first half of the 21st century. To better see the evolution of the Antarctic O_3 hole, we show the mean O_3

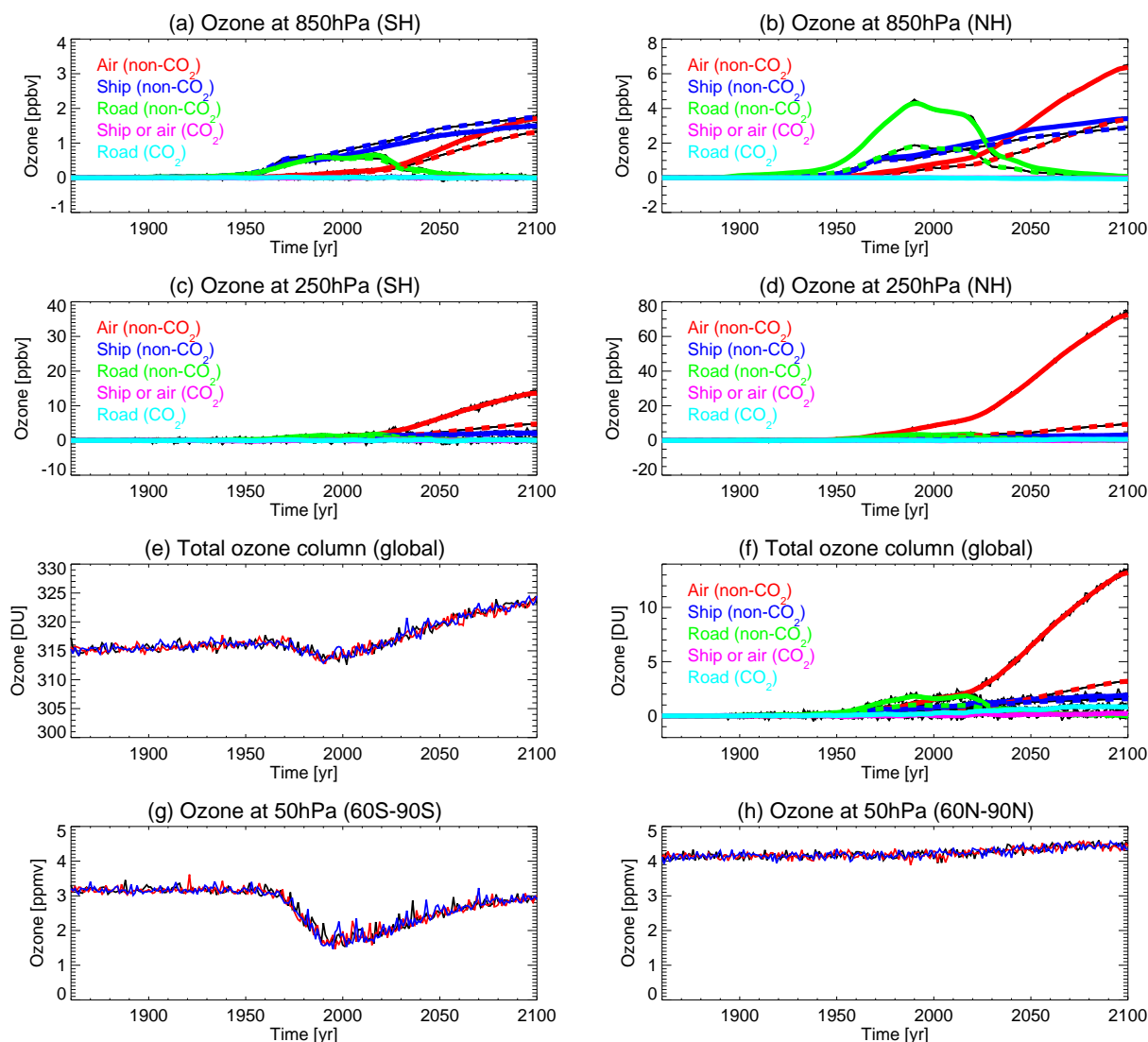


Fig. 6. Time series of the O_3 evolution: impact from the transport sectors on the O_3 mixing ratio at 850 hPa in the (a) SH and (b) NH, and at 250 hPa in the (c) SH and (d) NH; total O_3 column (e) in the reference simulation and (f) impact from the transport sectors; (g) O_3 mixing ratio in the reference simulation at 50 hPa averaged over the $60\text{--}90^\circ\text{S}$ region in September and (h) over the $60\text{--}90^\circ\text{N}$ region in March. In (a), (b), (c), (d) and (f), full lines indicate the dynamical O_3 approach and dashed lines the fixed O_3 approach. In (e), (g) and (h), the three different lines (black, red and blue) represent the three different members of the ensemble.

concentration at 50 hPa averaged over $60\text{--}90^\circ\text{S}$ in September in Fig. 6g and over $60\text{--}90^\circ\text{N}$ in March in Fig. 6h for the 3 members of the reference simulations. One sees an important decrease in the $60\text{--}90^\circ\text{S}$ O_3 concentration in 1990–2010, with an almost complete recovery up to pre-1960 values in 2070–2080. This agrees rather well with results from AGCMs with full stratospheric chemistry (WMO, 2010).

CO_2 emissions from transport also have some effect on the total O_3 column (Fig. 6f), probably due to a cooler stratosphere: there is a small increase at the end of the 21st century of around 1 DU due to road transport (light blue line), and less than 0.5 DU due to shipping or aviation (purple line).

These changes are in agreement with the total anthropogenic impact. For the non- CO_2 impact from aviation, the evolution of the O_3 column clearly shows again the strong difference between the perturbations due to the non- CO_2 (full line) and the non- CO_2^* (dashed line) approaches.

3.2 TOA forcing

For CO_2 , CH_4 , CFC-12 and HFC-134a, the radiative forcings from the transport sectors were presented in Fig. 1c–e. Here we present the TOA radiative forcing caused by O_3 (fixed O_3 approach), contrails and aerosols. To obtain these values

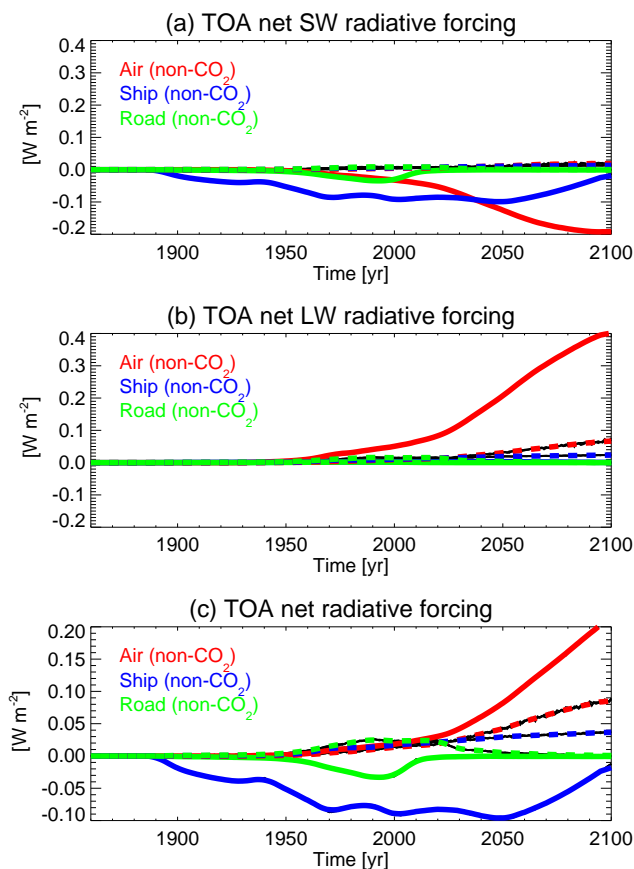


Fig. 7. Time series of annual global mean impact of O₃, aerosols and contrails on TOA (a) shortwave, (b) longwave and (c) net radiative fluxes from road transport (green), maritime shipping (blue) and aviation (red). The impact from O₃ (from the fixed O₃ approach) is indicated by the dashed lines, while the impact from aerosols and contrails together is indicated by the full lines.

for the period 1860–2100, we perform the radiative transfer calculation twice, once with the transport induced perturbation agents, and once without them (for the dynamical O₃ approach this is not possible). The difference gives the radiative imbalance induced by the forcing agent. With this method we obtain from the non-CO₂ simulations the summed impact from contrails and aerosols, and from the non-CO₂* simulations the summed impact from O₃, contrails and aerosols. By taking the difference between these approaches one can also derive the fixed O₃ impact.

Figure 7 shows the net TOA radiation impact from the O₃ forcing (dashed line) and from the combined aerosol and contrail forcing (full line). The O₃ impact in 2000 is 23.5, 16.8 and 13.5 mW m⁻² for road transport, shipping and aviation, respectively, and evolves in 2100 to 0.7, 36.5 and 85.3 mW m⁻². Although the NO_x emissions in 2100 are still considerably lower for aviation than for shipping, their radiative impact is considerably stronger – the radiative impact of both sectors is of similar size around 2020–2030. Surpris-

ingly the values for the year 2000 are lower than the values from Hoor et al. (2009, their Table 8), especially when one takes into consideration their lower road transport and aviation emissions: they found 27.9, 27.3 and 16.3 mW m⁻² for road transport, shipping and aviation, respectively. Our values are also smaller than the ones in Myhre et al. (2011) who found 31, 24 and 17 mW m⁻². The discrepancy can be partially caused by differences in the radiation scheme. For road transport, shipping and aviation, the impact from aerosols and contrails is found to be –28.4, –89.0 and 18.3 mW m⁻² respectively in the year 2000. These values correspond reasonably well with the results for aerosols and contrails in Sects. 2.2.5 and 2.2.6. As the forcing from BC is very small in our model, we find the total impact from road transport aerosols to be negative (this contrasts with Fuglestad et al., 2008; Balkanski et al., 2010; Uherek et al., 2010). The value for aviation is the sum of the positive impact from contrails and the negative impact from sulfate. In 2100 we find forcings of –0.7, –18.1 and 209 mW m⁻² for road transport, shipping and aviation, respectively. The strong decrease in the SO₂ emissions of shipping in the last 50 yr of the 21st century leads to this strongly reduced forcing in 2100.

In Fig. 8 we show global maps of the net TOA radiative impact from O₃ perturbations (rows a, b and c) and from aerosol and contrail perturbations (rows d, e and f). The O₃ perturbations are more zonally homogeneous than the summed aerosol and contrail perturbations, and for aviation we see the strongest impact between 10 and 40°N. When focussing on the aerosol and contrail impacts, we also see for road a negative impact caused by sulfate (due to underestimation of the BC impact). The impact is clearly stronger in the northern hemisphere (NH). For shipping, the strongest impact is over the NH oceans, and this perturbation is clearly greatest in the periods 1980–1999, 2011–2030 and 2046–2065, in agreement with the time series of SO₂ emissions. For aviation, the strongest positive impact is seen over the most frequently used aircraft routes in the NH. In regions of low air traffic however, we see some areas where the impact on TOA radiation is negative. This is clearest in the period 2046–2065 in the NH over the Arctic, and over the subtropical Atlantic and Pacific. As we do not find any of these signatures in simulations that included contrails only (not shown), we attribute the local negative forcing to sulfate. Sulfate has a clear signature in the Arctic (see the aviation sulfate distribution in Fig. 3c), is mainly confined to the NH and peaks around the year 2050. As the lifetime of contrails and SO₂/sulfate are different, one can have different distributions for their radiative forcing. Moreover the contrail and sulfate distributions result from two distinct CTMs, driven by different ECMWF analyses.

3.3 Surface air temperature

Figure 9a shows time series of the global annual mean of the surface air temperature for the three members of the

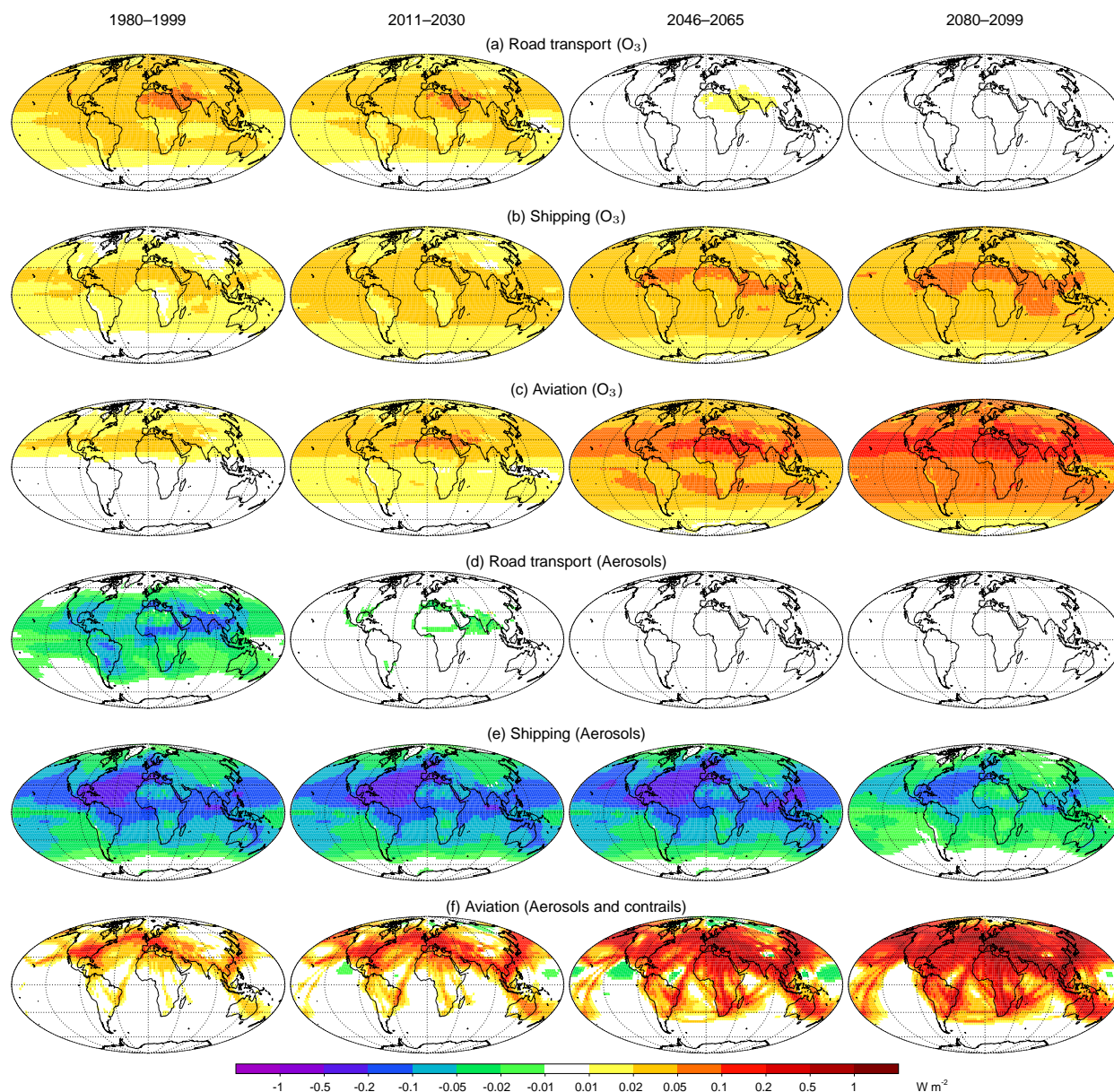


Fig. 8. Global maps of the annual mean impact on the net TOA forcing in the periods 1980–1999, 2011–2030, 2046–2065 and 2080–2099 by O_3 perturbations from (a) road transport, (b) maritime shipping and (c) aviation, by aerosols from (d) road transport and (e) maritime shipping, and (f) by aerosols and contrails from aviation.

reference simulation. Around the year 2000, the temperature increase is around 0.8 K w.r.t. 1860, increasing by almost 3.0 K in 2100. One notices that the three members of the ensemble show a very similar behavior. Using the results from the pre-industrial and doubled CO_2 simulation, we can determine the climate sensitivity using the method of Gregory et al. (2004) and find a value of around $0.8 \text{ K} (\text{W m}^{-2})^{-1}$, which corresponds with a 2.97 K temperature increase for a doubling of the CO_2 concentration. This is well within the interval mentioned in IPCC (2007) of 2.1 to 4.4 K with a mean value of 3.2 K.

Figure 9b shows time series of the impact of the transport sectors on the evolution of the global annual mean of the surface air temperature. The thin black lines show the annual global mean impact for the individual members of the ensemble, and the thick colored lines show the 11-yr running mean, averaged over the 3 ensemble members. For CO_2 the impact of road transport is strongest, showing a temperature increase of around 0.05 K in 2000, reaching 0.3 K in 2100. For aviation and shipping, the temperature impact until 2050 is small, reaching 0.1 K in 2100. The non- CO_2 impact from road is strongest between 2000 and 2050 (around

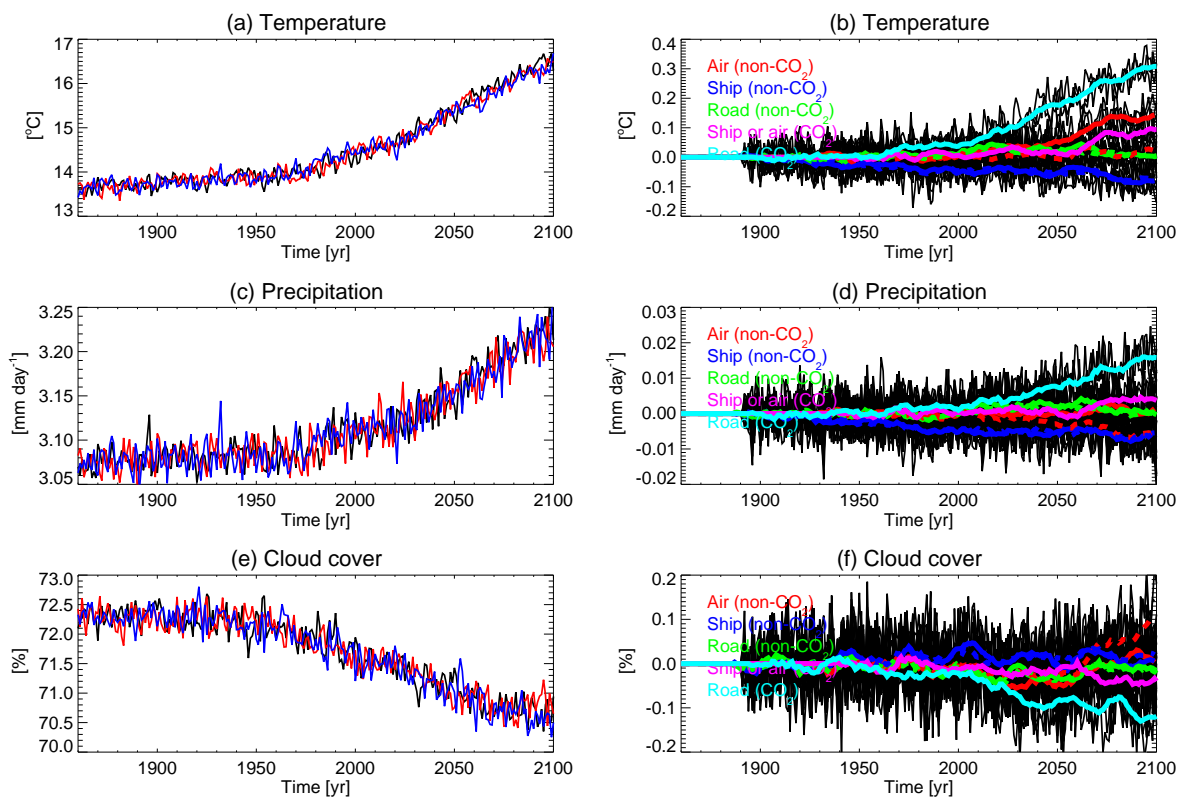


Fig. 9. Left: time series of annual global mean (a) surface air temperature, (c) precipitation, and (e) cloud cover over the period 1860–2100 taking into account the total anthropogenic forcing. The three different lines (black, red and blue) represent the three different members of the ensemble. Right: time series of impact on (b) surface air temperature, (d) precipitation, and (f) cloud cover by road transport, shipping and aviation, separately for their CO₂, non-CO₂ and non-CO₂* impact (the non-CO₂* impact is indicated by the dashed lines). The thin black lines indicate the individual impact from each of the three members of the simulation, and the thick lines indicate the 11-year running average of the ensemble mean.

0.05 K), and reduces thereafter. This is mainly caused by a strong reduction in the road transport emissions of NO_x in the second half of the 21st century and of the earlier reductions in the emission of CFC-12 and HFC-134a. Taking into account a stronger impact of BC would probably strengthen this behaviour. The non-CO₂ emissions from shipping show a negative impact on the temperature of around -0.05 to -0.1 K over the period 2000–2100. This is caused by significant SO₂ emissions leading to the formation of sulfate aerosols, together with a strong impact of OH on CH₄ by, on the one hand, significant NO_x emissions, and on the other hand, a characteristic strong impact of NO_x shipping emissions on the CH₄ lifetime (Hoor et al., 2009). For the non-CO₂ impact from aviation we see a strong difference between the non-CO₂ and non-CO₂* approaches, caused by the rather different O₃ perturbations (see Fig. 6). The non-CO₂ approach shows a positive impact reaching 0.15 K in 2100. This is caused by the strong increase in the NO_x aviation emissions that are more than 2.5 times more efficient than the other transport emissions at producing O₃ (see Hoor et al., 2009), and by the impact from the linear contrails and

aviation-induced cirrus. However, in the extended linear O₃ scheme the O₃ production in the upper troposphere seems to be overestimated (see Sect. 3.1). Using the non-CO₂* approach leads to almost no temperature signal, except for a very small increase in the last part of the 21st century. Both approaches probably are affected by the too strong negative forcing from sulfate aerosols (see Sect. 2.2.6). Taking this into consideration together with the fact that the model is not very sensitive to O₃ perturbations (see Sect. 2.2.4), we assume that the actual impact from aviation will be somewhere in between the results for both approaches.

Sausen and Schumann (2000) made projections of the impact of aviation on the global mean surface air temperature. They included the impact from CO₂ and O₃ changes due to NO_x emissions but not the impact from the reduction in the CH₄ lifetime or the impact from contrails or aviation-induced cirrus. One should also note that the climate sensitivity of their SCM was rather low, i.e. $0.61 \text{ K (W m}^{-2}\text{)}^{-1}$. They found a temperature increase of 0.006 K in 2000, and for their scenarios Fa1, Eab and Eah, respectively 0.025, 0.033 and 0.050 K in 2050 and 0.047, 0.086 and 0.146 K in

2100. We find in 2100 a total impact from aviation of around 0.25 K for the non-CO₂ approach and around 0.15 K using the non-CO₂* approach. Skeie et al. (2009) performed simulations with a more evolved SCM, using the SRES scenarios A1B, A2, B1 and B2, and calculated the combined CO₂ and non-CO₂ impact on surface air temperature for the different sectors. With a climate sensitivity of 0.8 K (W m⁻²)⁻¹, they found for the A1B scenario, an annual global mean surface air temperature impact in 2100 of 0.38 K for road, 0.02 K for shipping, and 0.28 K for aviation, which is in rather good agreement with our results. They used similar emission scenarios, however they took into account more forcings (stratospheric water vapour feedback, methane ozone feedback, ...). Berntsen and Fuglestedt (2008) did a similar study but only looked at the present-day impact.

We now focus on the geographical distribution of the surface air temperature impact. In Fig. 10 we present the annual mean changes averaged over the periods 1980–1999, 2011–2030, 2046–2065 and 2080–2099 from the total anthropogenic impact (row a) and from the separate transport impacts (rows b–g). Note the difference in the contour intervals between the first row and the other rows. For the total anthropogenic impact, a clear signal can already be seen in 1980–1999, which increases gradually until 2080–2099. Continents show a considerably stronger impact than oceans, and the temperature over the Labrador Sea shows an even stronger negative temperature response in 2046–2065 and 2080–2099. In the Southern Ocean, we also find a weak warming. A strong impact is also noticeable poleward of 65° N. These results compare well with results shown in IPCC (2007, Fig. 10.8).

For the road sector, we find a significant CO₂ impact of 0.2 K over continents for 2011–2030, with some regions showing increases of more than 0.4 K in 2080–2099. Large similarities with the total anthropogenic impact exist, e.g. the stronger impact at high northern latitudes and the stronger impact over continents. For the CO₂ impact from shipping and aviation, increases of 0.2 K over continents are seen in 2080–2099. The non-CO₂ impact for road transport is slightly positive in 2011–2030 and 2046–2065, whereas that from shipping is clearly negative and rather constant over the 21st century, with some extremes over the continents and over the northern high latitude regions. Using the non-CO₂ approach, the impact from aviation is clearly positive by 2011–2030, and a steady increase is seen for the periods 2046–2065 and 2080–2099 especially in the NH. However, using the non-CO₂* approach, we observe a clearly positive signal over the NH mid-latitudes only in 2080–2099.

In order to investigate the latitudinal dependence of the impacts, we show the annual zonal-mean surface air temperature in Fig. 11a. Results are shown for the periods 1980–1999, 2011–2030, 2046–2065 and 2080–2099, and are the mean of the 3 members over the 20-year periods. We also indicate the 95 % confidence intervals with thin lines. The zonal mean temperature response to the total anthropogenic

forcings shows a smaller impact at mid-latitudes (50–60° S, 40–50° N), but an amplification at the poles which is most pronounced in the Arctic. The confidence intervals are larger closer to the poles and smaller in the extra-tropics to mid-latitudes. Figure 11b–i shows the CO₂ and non-CO₂ impacts of the transport sectors on the annual zonal mean surface air temperature. The CO₂ impact from shipping and aviation only becomes clearly distinguishable in 2080–2099 (around 0.1 K in low and mid-latitudes), with a large amplification in the Arctic. The impact from road transport is stronger: at low latitudes, it is significant as from 2011–2030 (0.1 K), going up to 0.3 K in 2080–2099, and shows also a strong amplification in the Arctic. In contrast, the non-CO₂ impact from road in the tropics and at mid-latitudes is strongest in the periods 2011–2030 and 2046–2065 and has large confidence intervals in the Arctic and Antarctic. From shipping, the non-CO₂ impact is negative everywhere (except at southern high latitudes for the period 2011–2030 when it is weakly positive), with similar values in 2011–2030 and 2046–2065 in the tropics and extra tropics, and larger ones at northern high latitudes. The strongest non-CO₂ signal is from aviation with a very asymmetric response of up to 0.3 K in the region 20–60° N in 2100. The non-CO₂* approach however shows a much weaker signal, clearly positive between 20 and 50° N, but negative between 60 and 90° N. This local negative impact is possibly a consequence of the over-estimated sulfate (see the aviation sulfate distribution in Fig. 3c) and underestimated O₃ impacts.

To estimate the difference in geographical distribution of the impacts, we quantify the correlation between the patterns of climate change in the different periods shown in Fig. 10. For each impact in each period we calculate the correlation with the distribution that shows the strongest signal, i.e. the total anthropogenic impact in 2080–2099. Similar comparisons have been performed in IPCC (2007, Table 10.5), but using different measures (Watterson, 1996). Figure 12a shows these correlations for the surface air temperature distribution. One sees a strong correlation for the first 3 periods of the total anthropogenic impact, and for the CO₂ impact from road transport. Further, we see a negative correlation with the non-CO₂ impact from shipping. For the non-CO₂ impact from road, we see a positive correlation, which, however, disappears in 2080–2099.

In the sensitivity simulations, we amplified the forcings by a factor of five to derive the impacts from the different transport sectors. Whether such an amplification of the forcing is justified is determined by whether the perturbations are still small enough for the system to be in a linear regime (see Fig. 4). For the strongest perturbation (i.e. where we model the CO₂ impact from road) we can expect the strongest non-linearity. In the year 2100, we find an increase in global mean surface air temperature of 0.3 K due to the CO₂ emissions from road transport. This means that the actual temperature difference between the simulations is around 1.5 K, which is large w.r.t. a total climate change of around 3 K. To

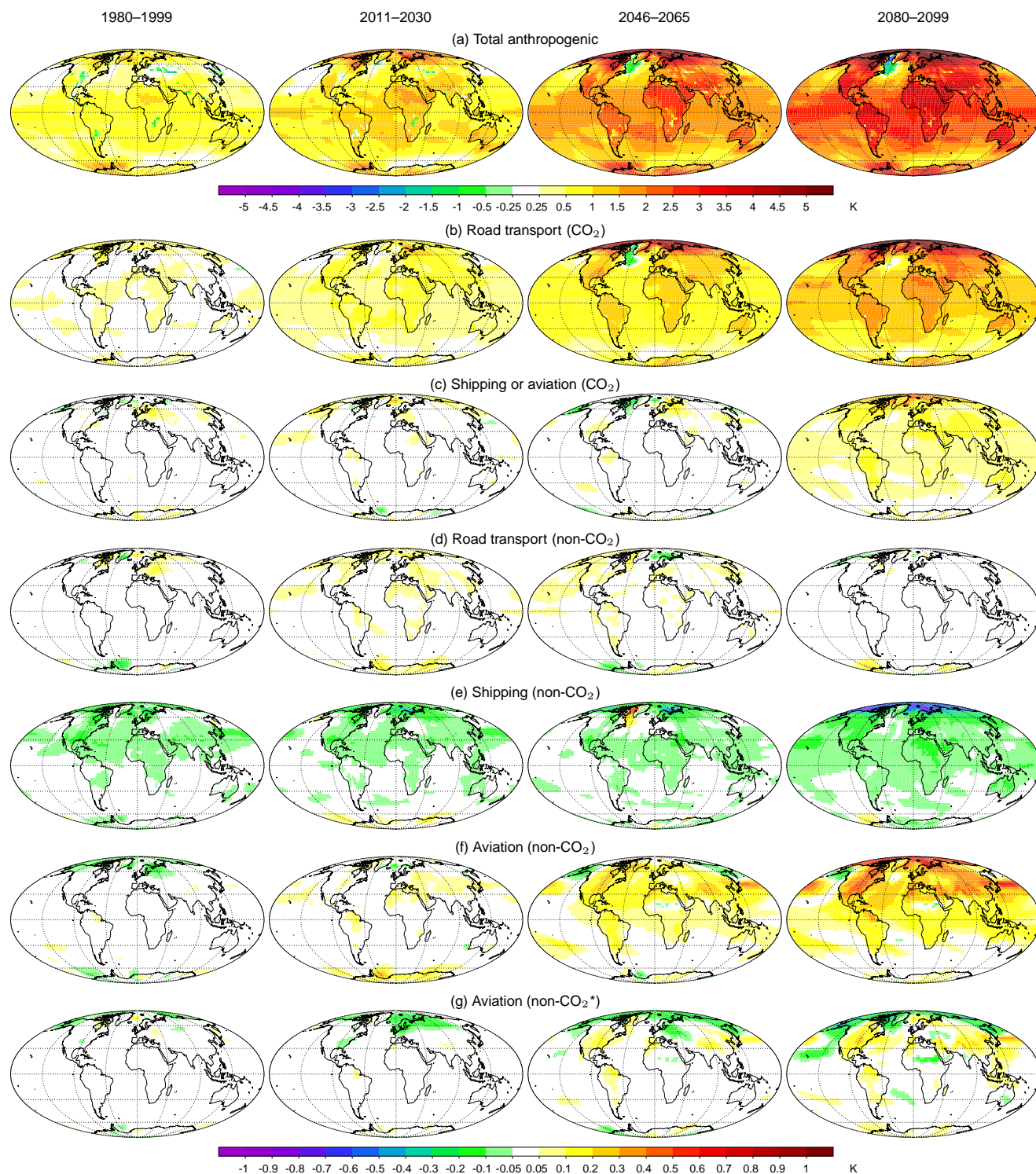


Fig. 10. Global maps of the annual mean surface air temperature impact in the periods 1980–1999, 2011–2030, 2046–2065 and 2080–2099 caused by (a) the total anthropogenic forcing, the CO₂ forcing from (b) road transport and (c) shipping or aviation, by the non-CO₂ forcing from (d) road transport, (e) shipping and (f) aviation where we use the dynamical O₃ approach to take into account the effect of O₃, and (g) by the non-CO₂* impact from aviation (using the fixed O₃ approach). Notice that the contour intervals are 5 times larger for the total anthropogenic perturbation (a).

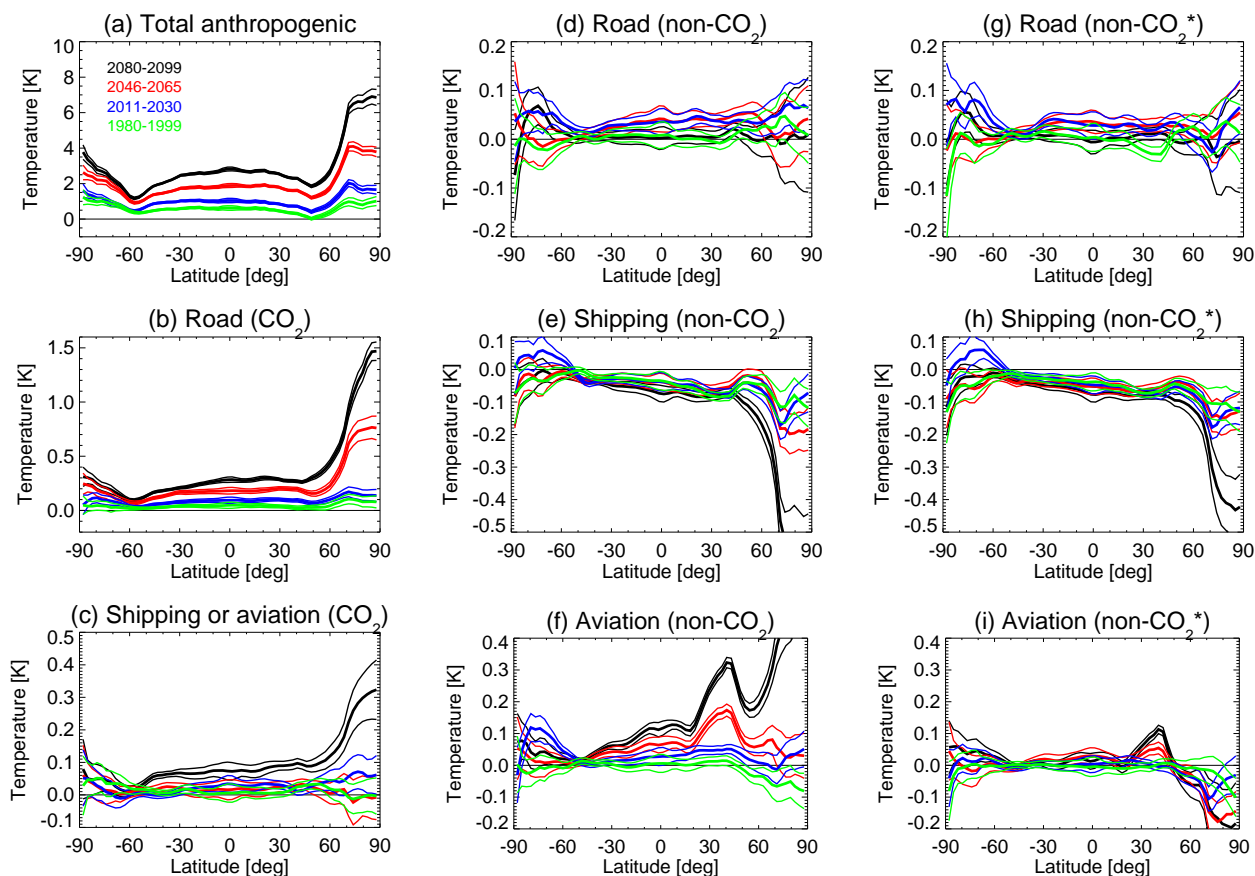


Fig. 11. Annual zonal mean surface air temperature impact in 1980–1999 (green), 2011–2030 (blue), 2046–2065 (red) and 2080–2099 (black): (a) total anthropogenic impact, CO₂ impact from (b) road transport and (c) shipping or aviation, non-CO₂ impact using the dynamical O₃ approach for (d) road transport, (e) shipping and (f) aviation, and non-CO₂* impact using fixed O₃ approach for (g) road transport, (h) shipping and (i) aviation. Thick lines are the mean over the 3 members and thin lines indicate the 95 % confidence interval.

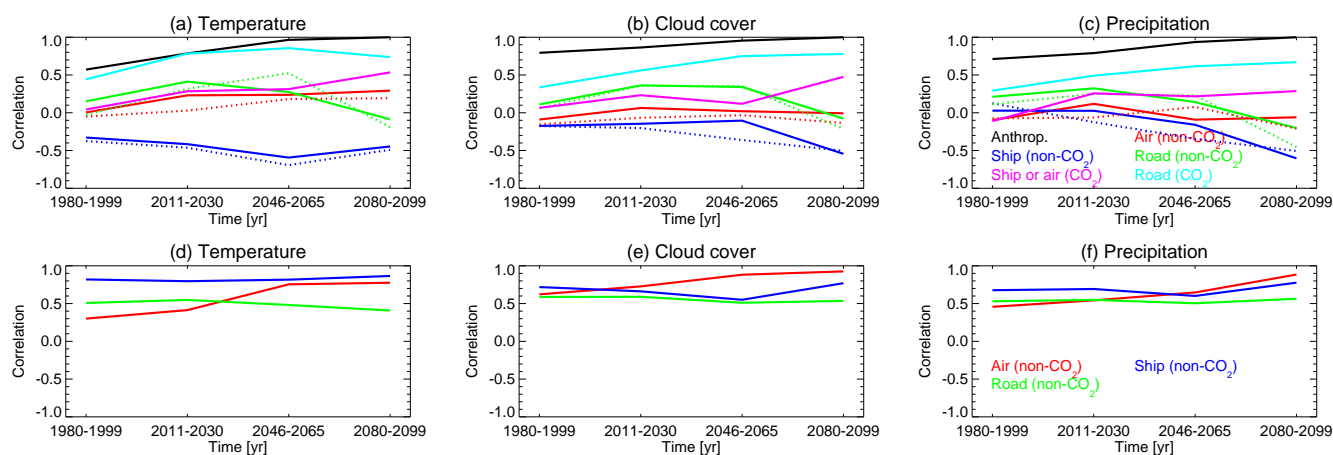


Fig. 12. First row: correlation between the impact on the geographical distributions of annual mean (a) surface air temperature, (b) cloud cover and (c) precipitation from a perturbation in a certain period with the total anthropogenic impact of the period 2080–2099. The dotted lines show the result for the fixed O₃ approach. Second row: correlation between the two different non-CO₂ approaches (fixed O₃ versus dynamical O₃ approach) for (d) surface air temperature, (e) cloud cover and (f) precipitation.

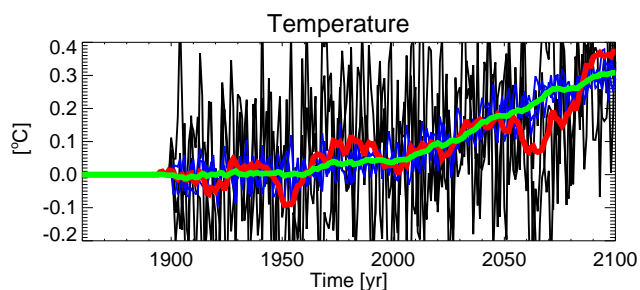


Fig. 13. Time series of the annual global mean surface air temperature over the period 1860–2100: black (scaling 1), red (scaling 1, 11-yr running average), blue (scaling 5), and green (scaling 5, 11-yr running average).

obtain the CO₂ impact from road transport, we thus compare a simulation containing 5 times the CO₂ emissions from road transport (red line in Fig. 4) with a simulation with no CO₂ emissions from road transport (blue line). The CO₂ impact from road transport can also be analyzed using the difference between the reference simulation (black line) and the simulation with no CO₂ emissions from road (blue line). Figure 13 shows the evolution of the annual global mean surface air temperature for both approaches. The approach without amplification of the forcing gives a much noisier result, with a high inter-annual variability, while the approach with a 5 times stronger forcing shows a much more stable signal and a suppressed variability, but on average both approaches coincide. Figure 14 shows the impact on the zonal mean surface air temperature from both approaches for the periods 1980–1999, 2011–2030, 2046–2065 and 2080–2099. There, one sees that both approaches agree in the tropics up to the mid-latitudes rather well, but that at high latitudes the differences are larger. The 95 % confidence interval is considerably smaller for the simulations where we apply 5 times the actual forcing.

3.4 Atmospheric temperature profile

Figure 15a shows the total anthropogenic impact on the annual zonal mean temperature profile for the periods 1980–1999, 2011–2030, 2046–2065 and 2080–2099 w.r.t. the pre-industrial simulation. Strongest values appear in the low-latitude mid- and upper-troposphere, up to 1, 1.5, 3.5 and 5 K for the respective 4 periods, which correspond well with those in IPCC (2007, Fig. 10.7). The impact at the surface is smaller and shows more variability. Figure 15b–c shows the impact on the annual zonal mean temperature profile by CO₂ from road transport and maritime shipping or aviation. The CO₂ impact from road transport is much stronger than that from shipping or aviation. In the mid- to upper-troposphere it varies around 0.05, 0.15, 0.35 and 0.5 K in 1980–1999, 2011–2030, 2046–2065 and 2080–2099, respectively. For shipping and aviation, there is no clear signal in 1980–1999,

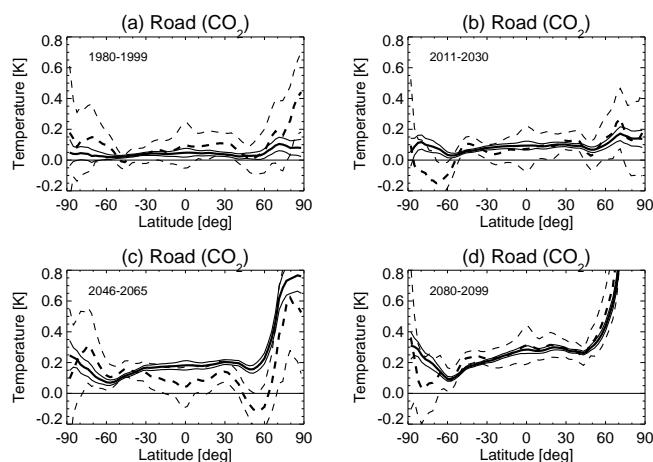


Fig. 14. Annual zonal mean surface air temperature impact from road transport for the periods (a) 1980–1999, (b) 2011–2030, (c) 2046–2065 and (d) 2080–2099 using scaling 1 (dashed lines) and scaling 5 (full lines). The thin lines indicate the 95 % confidence interval.

2011–2030 and 2046–2065 (although an indication of a low-latitude mid- to upper-troposphere temperature increase appears). In 2080–2099 this impact goes up to 0.15 K in the tropical upper troposphere.

The non-CO₂ impacts for the transport sectors are shown in Fig. 15d–g, with both non-CO₂ and non-CO₂* approaches shown for aviation. We observe a positive signal in 2011–2030 and 2045–2065 for road transport, and a smaller impact at the end of the 21st century. For maritime shipping, there is a distinctive negative impact over the whole depth of the troposphere which is strongest in 2080–2099. The non-CO₂ impact from aviation is clearly positive in the troposphere, and in contrast with that from road transport and maritime shipping, it is very asymmetric being much stronger in the NH with a maximum around 300 hPa at 30–60° N. Here, the temperature increases by more than 0.5 K in 2100. Using the non-CO₂* approach the general pattern is similar, although the heating is weaker and one observes a strengthened cooling around 200 hPa between 50 and 80° N. Moreover, a negative signal appears at the surface between 60 and 90° N. Using an AGCM coupled to a slab ocean model and the emission scenario Fa, Ponater et al. (2005) found a maximum zonal mean temperature impact from aviation for the year 2050 of 0.35 K around 40–50° N at 300–400 hPa.

3.5 Precipitation and cloud cover

Time series of cloud cover and precipitation can be found in Fig. 9c–f. Taking into account the total anthropogenic impact, the precipitation rises by 0.2 mm day^{−1} in 2100, while the cloud cover decreases by 1.8 %, coinciding with the increase in global mean surface air temperature. A similar relationship is seen for individual transport sectors, although

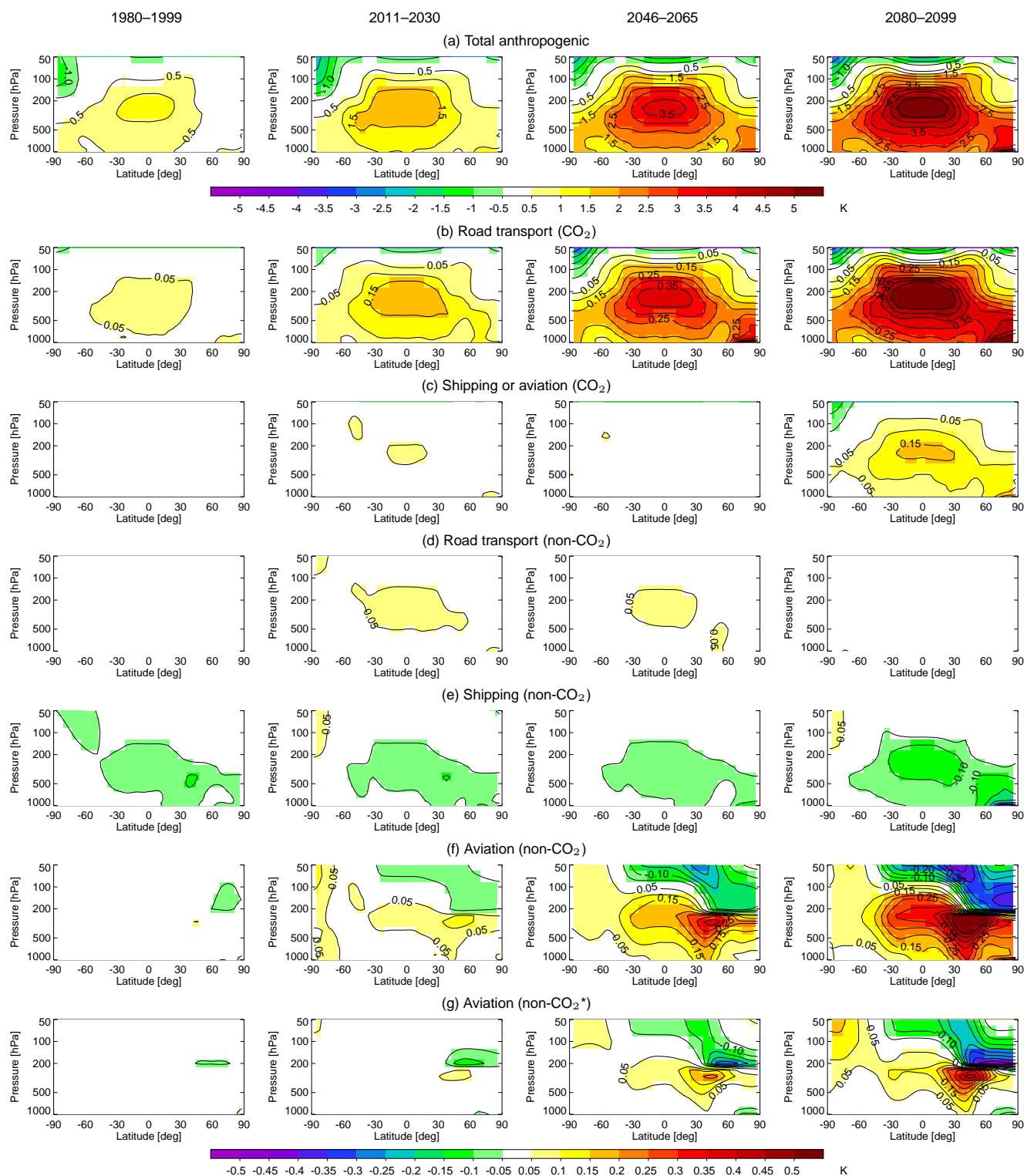


Fig. 15. Impact on annual zonal mean temperature profile in the periods 1980–1999, 2011–2030, 2046–2065 and 2080–2099. The order of the plots is as in Fig. 10. Notice that the contour intervals are 5 times larger for the total anthropogenic perturbation (a).

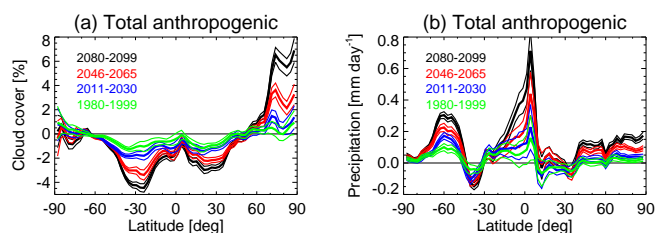


Fig. 16. Zonal annual mean (a) cloud cover and (b) precipitation change in 1980–1999 (green), 2011–2030 (blue), 2046–2065 (red) and 2080–2099 (black) from total anthropogenic forcing. The thick lines indicate the best estimate, the thin lines indicate the 95 % confidence interval.

for cloud cover the evolution is rather noisy. Largest impacts can be observed for CO₂ from road transport, showing in 2100 a 0.015 mm day⁻¹ increase in precipitation and a 0.15 % decrease in cloud cover. All other impacts are below 0.01 mm day⁻¹ for precipitation and 0.1 % for cloud cover.

To get an idea of the zonal mean distributions, we show the total anthropogenic impact in Fig. 16. The cloud cover remains almost unaffected in the tropics, decreases considerably in the subtropics, and has a strong increase at northern high-latitudes. These characteristics correspond well with those of IPCC (2007, Fig. 10.10). There is generally less confidence in the changes in precipitation but increases in precipitation at high latitudes are very consistent among models, and can also be observed in Fig. 16b. Our model also shows a decrease in subtropical regions.

In Fig. 12b–c, we show the correlation between the patterns of precipitation or cloud cover with the total anthropogenic impact in 2080–2099 (as for the surface air temperature). The results are similar to those for surface air temperature but in general the correlations are weaker, e.g. the non-CO₂ impact from shipping shows a strong anti-correlation only for the period 2080–2099. The behavior of the non-CO₂ impact from aviation is very different: there is no correlation neither for cloud cover nor for precipitation.

3.6 North Atlantic Oscillation

Figure 17a shows time series of the North Atlantic Oscillation (NAO) index over the period 1860–2100 taking into account the total anthropogenic impact. NAO anomalies represent the Lisbon (38.7° N, 9.1° W) minus Reykjavik (65.1° N, 22.7° W) normalized December–March average sea level pressure anomalies, with 1971–2000 as reference. One can observe a weak positive trend. Figure 17b shows the mean impact over the period 2050–2099 from the different transport sectors on the NAO index. The CO₂ impact is positive, road impact being around 20 % of the total anthropogenic one, and shipping or aviation being 5 %. For the non-CO₂ and non-CO₂* cases, we find small impacts for shipping and road transport, but a relatively strong one for aviation, both for the non-CO₂ and non-CO₂* approaches.

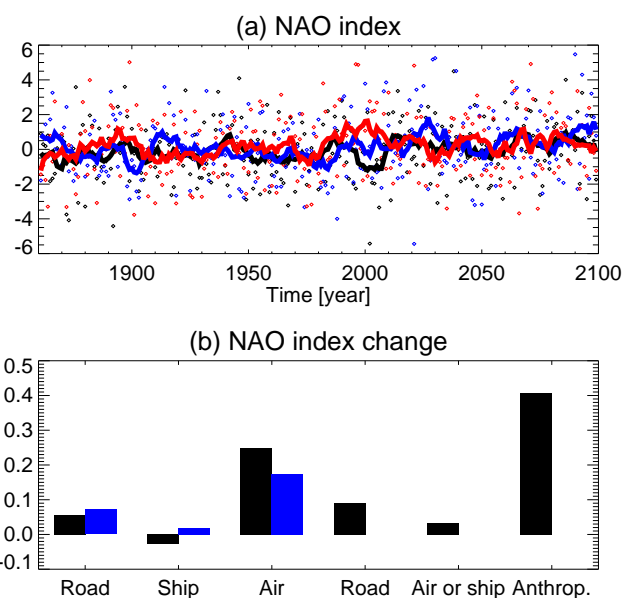


Fig. 17. (a) Mean NAO anomalies calculated from sea level pressures taking into account the total anthropogenic impact (the different colors indicate the 3 simulations of the ensemble). Single dots indicate yearly values, and lines show 11-yr running averages. (b) Impact of the transport sectors on the NAO anomaly averaged over 2050–2099. The first three bars show the non-CO₂ (black) and non-CO₂* (blue) impacts, the following two the CO₂ impacts, and the last one the total anthropogenic impact.

4 Ocean

In this section we describe the impact from the different transport sectors on ocean temperature, sea level, MOC, sea-ice extent and the Ni  o 3.4 index.

4.1 Ocean temperature

Figure 18 shows zonally averaged impacts on ocean temperature to a depth of 4000 m for the same periods as for the atmosphere, i.e. 1980–1999, 2011–2030, 2046–2065 and 2080–2099. Figure 18a shows the total anthropogenic impact. For all periods one observes a heating of the southern ocean, and the strongest impact can be seen in the southern mid-latitudes where the heating signal easily penetrates down to 3500–4000 m. At low latitudes, one sees initially (1980–1999 and 2011–2030) a cooling of the waters between 300 and 2000 m, probably caused by reduced mixing in response to more stable temperature profiles. Figure 18b–g shows the impacts from the transport perturbations: the CO₂ impact from road transport is the most important, while the non-CO₂ emissions from shipping have a cooling impact. The non-CO₂ effects of aviation have their greatest impact in the NH.

Figure 19 shows the zonally averaged increase in the heat content in the ocean integrated over the whole depth of

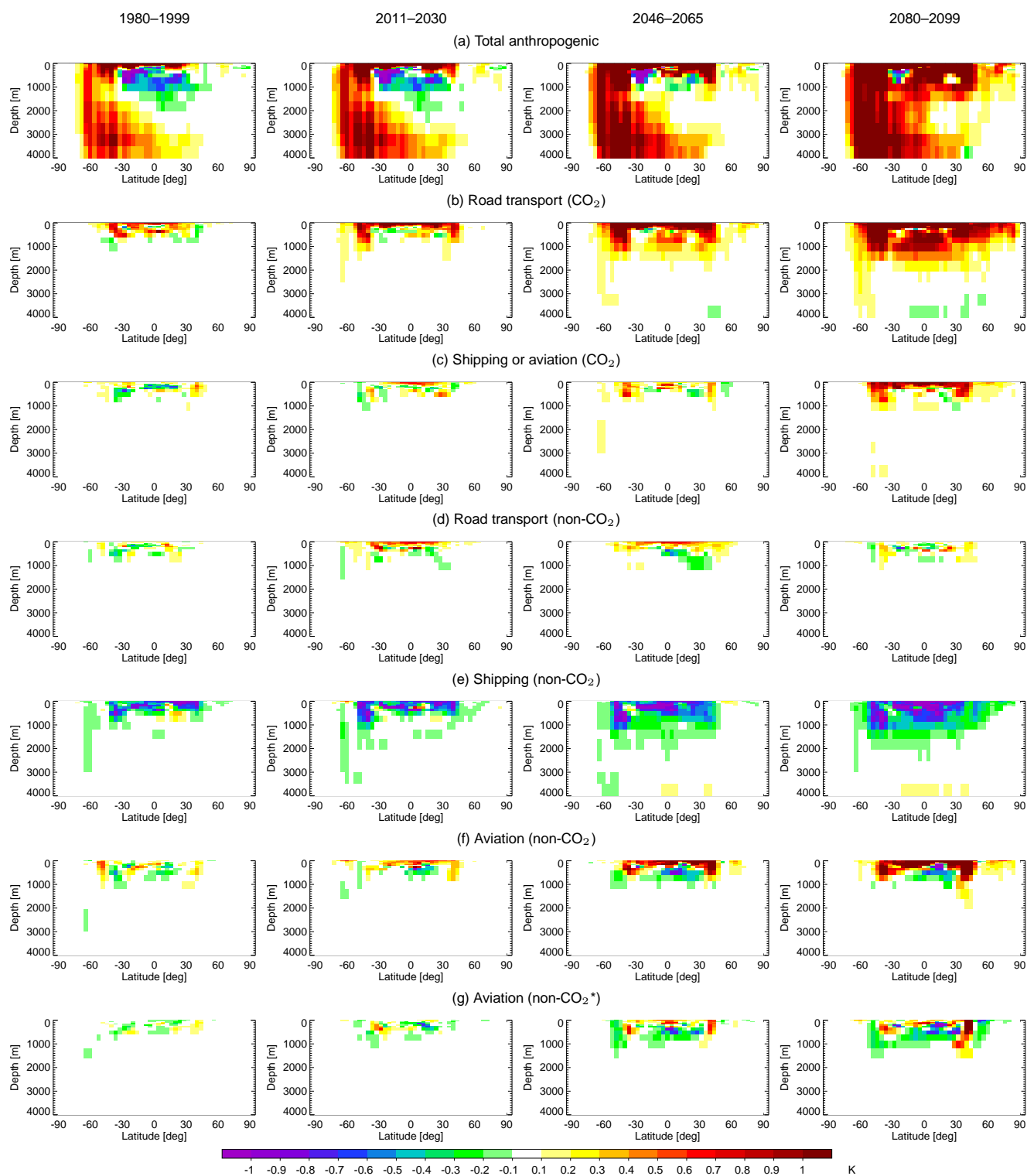


Fig. 18. Zonally averaged annual mean impact on the ocean temperature (in K) for the four different reference periods. The order of the plots is as in Fig. 10.

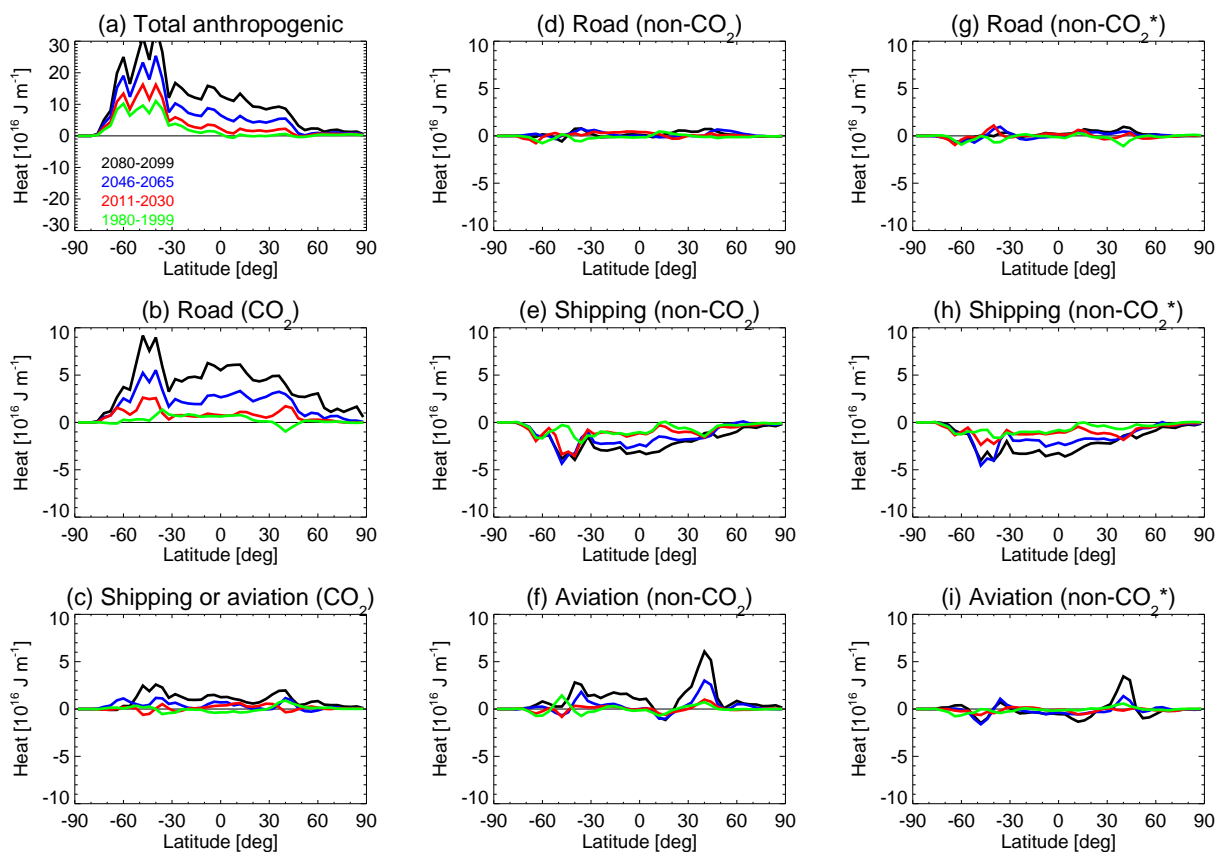


Fig. 19. Zonally integrated heat uptake by the ocean (in 10^{16} J m^{-1}) in 1980–1999 (green), 2011–2030 (blue), 2046–2065 (red) and 2080–2099 (black). The order of the plots is as in Fig. 11.

the ocean (in 10^{16} J m^{-1}). The total anthropogenic impact (Fig. 19a) shows two characteristic features: most of the heat is stored in the southern ocean, while almost no heat is stored north of 45° N , and the increase is very regular over the 4 periods. The CO_2 impacts from road transport, shipping or aviation present similar features. For the non- CO_2 impact, we notice the small values for road transport, the negative impact for shipping, and the large heating between 25 and 50° N for aviation in the non- CO_2 approach, larger than that of the non- CO_2^* approach concentrated between 30 and 50° N .

Time series of the global mean ocean temperature can be seen in Fig. 20a–b. One notices that these time series are rather smooth and show less inter-annual variability than the time series of the surface air temperature (see Fig. 9a–b). The non- CO_2 impact from shipping is negative, and prevails over the non- CO_2 impact from aviation and the CO_2 impact from shipping or aviation – a fact which is not clear for the surface air temperature evolution. Another interesting feature is the significant difference for shipping between the non- CO_2 and non- CO_2^* approaches in the second half of the 21st century.

4.2 Sea level

Sea level rise in a changing climate results from thermal expansion of the oceans as well as from melting of glaciers, ice caps and the Greenland and Antarctic ice sheets. Figure 20c–d shows the sea level rise (in mm) that includes only the thermal expansion of the oceans calculated from the standard expression for the density as a function of pressure, temperature and salinity in Millero and Poisson (1981). The total anthropogenic induced rise in sea level is 30 mm in 2000 and increases to 180 mm in 2100. The CO_2 impact from road is around 18 mm in 2100. The strongest non- CO_2 impact results from shipping, causing a 3 mm decrease in 2000 and almost 8 mm in 2100. The CO_2 impact from shipping or aviation and the non- CO_2 impact from aviation are similar, leading to a rise in sea level of around 4 mm in 2100. The non- CO_2^* approach for aviation shows almost no impact.

IPCC (2007) report a sea level rise due to thermal expansion of between 130 and 320 mm (anthropogenic impact in 2090–2099 relative to 1980–1999, scenario A1B), and between 210 and 480 mm for the total sea level rise. This indicates that thermal expansion contributes to more than 50 % of the total rise in sea level, and shows that our results are at the low end of their range.

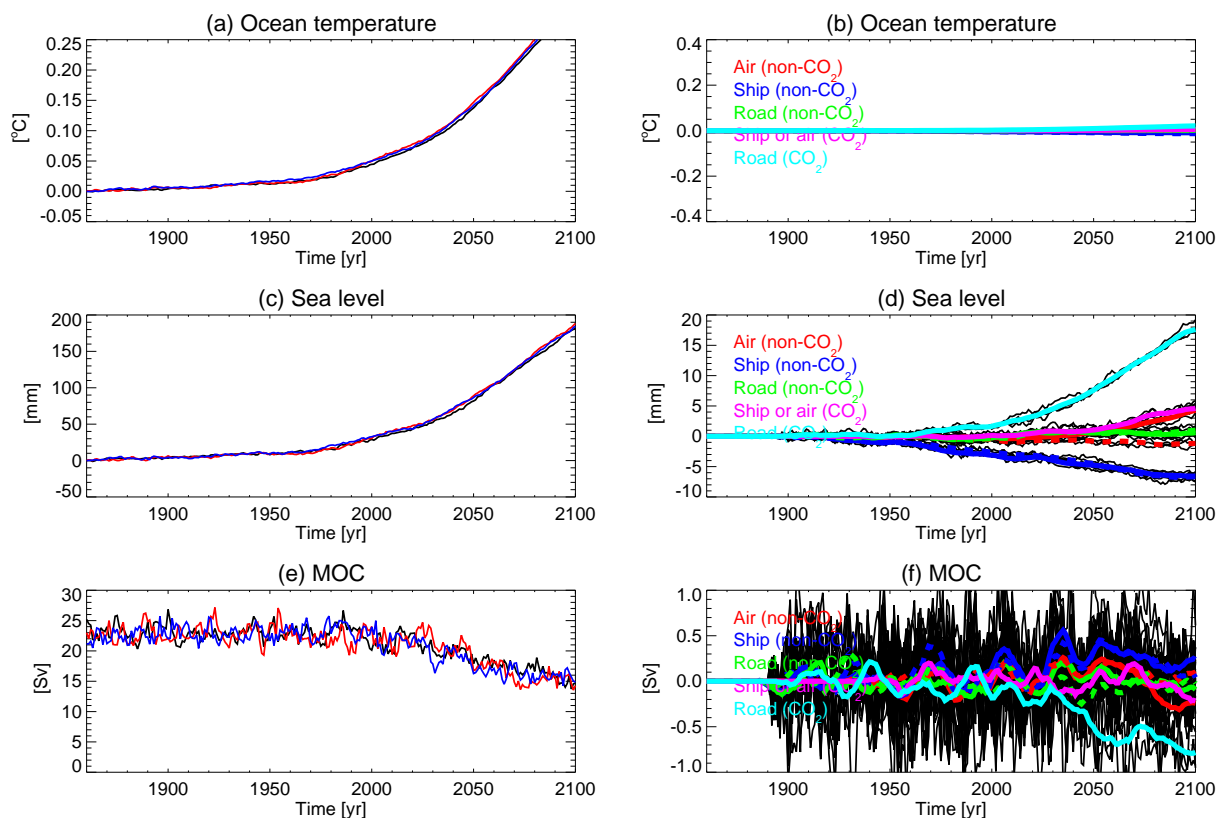


Fig. 20. Left: time series of total anthropogenic impact on (a) the ocean mean temperature, (c) sea level and (e) meridional overturning circulation. The three different lines (black, red and blue) represent the three different members of the ensemble. Right: the impact by road transport, shipping and aviation, separately for their CO₂, non-CO₂ and non-CO₂* impact (the non-CO₂* impact is indicated by the dashed lines) on (b) the ocean mean temperature, (d) sea level and (f) meridional overturning circulation. The thin black lines indicate the individual impact from each of the three members of the simulation, and the thick lines indicate the 11-yr running average of the ensemble mean.

Sausen and Schumann (2000) estimated the rise in sea level due to emissions from aviation. Their results were obtained using an SCM (see Sect. 3.3), whose calibration was based on an AOGCM that accounted for the rise in sea level due only to thermal expansion. They included the impact from melting ice-sheets by almost doubling the parameter responsible for the rise in sea level in the SCM. They found in 2100 increases in sea level by 6.5, 11.2 and 18.6 mm for their scenarios Fa1 (that best corresponds with our aviation emission scenario A1B), Eab and Eah, respectively, compared with our values of between 3.5 and 8.5 mm in 2100 due to thermal expansion only.

4.3 Meridional overturning circulation

Figure 20e shows the evolution of the MOC. It is calculated as the maximum of the depth integrated northward mass flux at 30° N in the Atlantic Ocean. As our ocean model grid is not regular in the NH, the location of the integration varies slightly between around 33 and 27° N. Compared with ocean temperature and sea level, there is a much stronger inter-annual variability. In our model, the MOC of the reference

simulation between 1860 and 1970 varies mainly between 21 and 25 Sverdrup (Sv), values slightly higher than late 20th century observations. In 2100, the model predicts a decrease of the MOC down to 13–15 Sv for the total anthropogenic impact. Our modeled slowdown of the MOC corresponds well with results obtained in IPCC (2007).

Figure 20f shows the transport impact on the MOC. The CO₂ road emissions lead to a decrease of 0.8 Sv in 2100, corresponding roughly to 10 % of the total anthropogenic impact. The non-CO₂ impact from shipping is positive, while all the other impacts are rather small.

4.4 Sea-ice

Figure 21a–d shows the impact on the sea-ice extent in the Arctic (in 10¹² m²) at the end of the winter (March) and at the end of the summer (September) from total anthropogenic influence (left) and from the transport sectors (right). It indicates that the maximum extent of the sea-ice cover in March is not affected very much by the changing climate, with quite good agreement among the different simulations. In September, however, the sea-ice cover decays strongly in the second

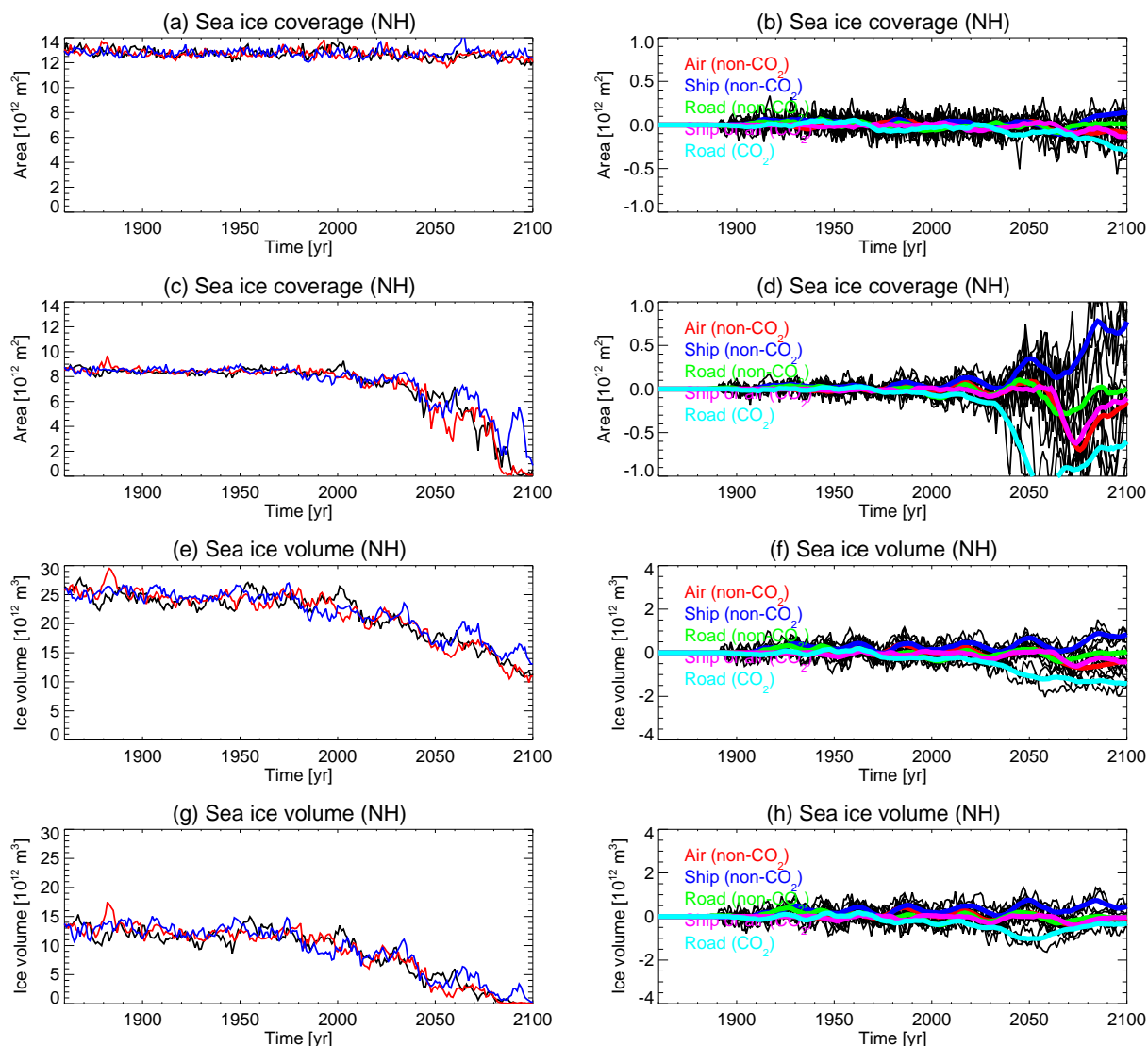


Fig. 21. Left: time series in the reference simulation of (a) NH sea-ice coverage (in 10^{12} m^2) in March, (c) NH sea-ice coverage in September, (e) NH sea-ice volume (in 10^{12} m^3) in March and (g) NH sea-ice volume in September. Right: the impact by road transport, shipping and aviation, separately for their CO_2 and non- CO_2 impact on (b) NH sea-ice coverage in March, (d) NH sea-ice coverage in September, (f) NH sea-ice volume in March and (h) NH sea-ice volume in September.

half of the 21st century, showing large variability within and among the different simulations. Importantly, two of the simulations have no sea-ice in 2100 in the Arctic in September. The large variability in the Arctic sea-ice cover corresponds with a large variability in the local surface air temperature.

From all transport sectors, we see small impacts in March and large impacts in September. In addition, the CO_2 impact in September from road transport is very different before 2050 compared with after. This is due to the fact that in the perturbed simulation there is no sea-ice in March from 2050 onwards, and the sensitivity is therefore reduced. The actual impact is therefore expected to be larger than indicated. Similar sudden changes can be seen around 2070 for the CO_2

impact from shipping and aviation, and for the non- CO_2 impact from aviation. Figure 21e–h shows the evolution of the sea-ice volume (in 10^{12} m^3) in the Arctic. Due to the total anthropogenic impact, the sea-ice volume decreases considerably in March in the 21st century, which was not the case for the sea-ice extent. Further, all transport sectors show the same reduced sensitivities in September at the end of the 21st century.

4.5 El Niño

In Fig. 22a we show the anomaly in the Niño 3.4 index (5-month running average sea surface air temperature over the

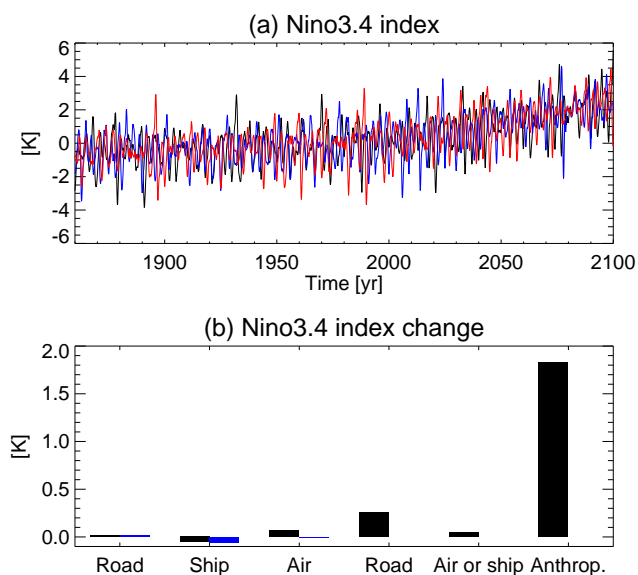


Fig. 22. (a) Evolution of the Niño 3.4 index anomaly over the 1860–2100 period for the 3 simulations forced by the total anthropogenic forcing (reference value calculated as the ensemble mean over 1971–2000). (b) Mean impact on the Niño 3.4 index of the different transport sectors over 2050–2099: the first three bars indicate the non-CO₂ impact (black for the dynamic O₃ approach, blue for the fixed O₃ approach), the following two bars the CO₂ impact, and the last bar the total anthropogenic impact.

domain 5° S–5° N, 120–170° W, Trenberth, 1997) for the reference simulations with the total anthropogenic impact. The reference period is 1971–2000. One sees that the anomaly in Niño 3.4 index increases in the 21st century. Figure 22b shows the impacts from transport on the Niño 3.4 index over the 2050–2099 period, and for reference the total anthropogenic impact is also indicated. The strongest impact is that from CO₂ from road transport, which contributes to around 15 % of the total. The non-CO₂ impact from shipping is negative, whilst for aviation, the non-CO₂* approach gives a considerably smaller impact than the non-CO₂ approach.

5 Conclusions

For the period 1860–2100 (SRES scenario A1B for 2000–2100), we have studied the impact of road transport, maritime shipping and aviation on climate with the atmosphere ocean general circulation model CNRM-CM3.3. This is one of the first studies with an AOGCM where the main forcings of the transport sectors are explicitly taken into account. We performed a reference simulation which represents the total anthropogenic impact and several sensitivity simulations to estimate the impact of the transport sectors. We separately estimated the impact from CO₂ and from non-CO₂ forcings. As non-CO₂ forcings, we included the impact of O₃, CH₄, aerosols, contrails, CFC-12 and HFC-134a. Most of the

emission inventories we used were the ones generated within the QUANTIFY project (<http://www.ip-quantify.eu>).

As a principal indicator of climate change we have looked at global mean impacts. In the reference simulation, we found an increase in annual global mean surface air temperature of around 0.8 K in 2000, reaching 3.0 K in 2100. In 2000, the CO₂ impact from all transport sectors together is of the order of 0.1 K. The emission of CO₂ from road transport contributes to a global mean warming of 0.3 K in 2100, while shipping and aviation each contribute to 0.1 K in 2100. The contribution of CO₂ from the transport sectors to the total anthropogenic temperature change increases from 12.5 % in 2000 to 16.7 % in 2100.

The non-CO₂ impact differs strongly among the different sectors. For road, this impact is largest between 2000 and 2050 (order of 0.1 K) becoming smaller at the end of the 21st century. The non-CO₂ impact from shipping is clearly negative reaching –0.1 K between 2050 and 2100, while from aviation it is positive but depends strongly on the treatment of the O₃ perturbations, reaching possibly 0.15 K in 2100. This indicates that during the period 1900–2100, the net impact of road transport on climate is positive and dominated by its CO₂ impact, the net impact of maritime shipping is mainly negative only becoming neutral at the end of the 21st century, while for aviation it is clearly positive and presumably dominated by its non-CO₂ emissions, even in 2100.

The use of an AOGCM also allows us to obtain geographical distributions of impacts. We observe an amplification of the surface air temperature signal at the poles, especially in the Arctic, both in the reference simulation, as well as in the sensitivity simulations. However, while for road and shipping the non-CO₂ impact on the surface air temperature is only slightly stronger in northern than in southern mid-latitudes, the impact for aviation can be up to a factor of 5 stronger in the northern hemisphere. The geographical pattern of the non-CO₂ climate impact for road transport and shipping coincides well with the total anthropogenic impact, while for aviation it is different. We also found a strong impact from the aviation non-CO₂ forcing on the NAO index.

Focussing on the ocean, we see that for the total anthropogenic impact and most of the transport impacts, the strongest deep ocean heating is observed in the southern mid-latitudes, while for aviation there is a significant response in the northern mid-latitudes. Further we find a rise in sea level due to thermal expansion in 2100 of 17.6 mm for road transport and 4.6 mm for maritime shipping and aviation. The rise due to non-CO₂ emissions in 2100 is of the order of 1 mm for road transport, –6.6 mm for maritime shipping and probably between –1.2 and 4.3 mm for aviation. This can be compared with a total anthropogenic impact in 2100 of around 180 mm. An overview of our principal results on surface air temperature and sea level rise can be found in Table 5.

In order to obtain detectable impacts, we used ensembles of 3 members together with a five-fold amplification of the

Table 5. Global mean surface air temperature change and sea level rise for selected years. The values are 11-yr means around the year mentioned, and averaged over the different members of the ensemble. The non-CO₂* forcing is as the non-CO₂ forcing except for O₃ where prescribed O₃ perturbation fields are used (see Sects. 2.2.4 and 3.1).

		Temperature [K]							Uncertainty
		1950	1975	2000	2025	2050	2075	2100	
Total anthropogenic		0.260	0.420	0.837	1.113	1.777	2.347	2.830	±0.060
CO ₂	Road transport	0.001	0.033	0.037	0.098	0.177	0.259	0.308	±0.012
	Shipping or aviation	−0.002	−0.003	0.007	0.029	0.013	0.084	0.094	±0.012
non-CO ₂	Road transport	0.001	0.007	0.012	0.033	0.020	0.008	0.003	±0.012
	Shipping	−0.024	−0.036	−0.053	−0.035	−0.053	−0.060	−0.076	±0.012
	Aviation	0.000	0.002	0.006	0.039	0.053	0.132	0.144	±0.012
non-CO ₂ *	Road transport	0.008	0.009	0.006	0.034	0.034	0.015	0.005	±0.012
	Shipping	−0.026	−0.041	−0.045	−0.044	−0.048	−0.066	−0.075	±0.012
	Aviation	−0.011	−0.002	0.003	0.007	−0.004	0.020	0.021	±0.012
		Sea level rise [mm]							Uncertainty
		1950	1975	2000	2025	2050	2075	2100	
Total anthropogenic		9.3	14.5	30.8	49.3	85.3	134.2	179.1	±0.8
CO ₂	Road transport	0.0	1.0	1.6	3.9	7.6	12.8	17.6	±0.2
	Shipping or aviation	−0.1	−0.2	0.1	0.7	1.0	3.2	4.6	±0.2
non-CO ₂	Road transport	0.1	−0.3	−0.3	0.6	0.6	0.4	0.6	±0.2
	Shipping	−1.0	−2.3	−3.1	−3.6	−4.8	−6.0	−6.6	±0.2
	Aviation	−0.1	−0.1	−0.2	−0.1	0.6	2.2	4.3	±0.2
non-CO ₂ *	Road transport	−0.1	−0.5	−0.4	0.8	0.6	0.5	1.0	±0.2
	Shipping	−1.1	−1.7	−2.6	−3.3	−4.6	−6.3	−6.6	±0.2
	Aviation	−0.1	−0.3	−0.5	−0.7	−0.8	−1.1	−1.2	±0.2

transport induced forcings. If the forcings had not been amplified, a larger and computationally more expensive ensemble would have been required. We found that the amplification of the forcing did not excessively disturb variables such as the surface air temperature. However, for quantities like sea-ice extent or sea-ice volume in the NH in September (a period when the sea-ice is very sensitive to variations in a non-linear way), the method has shown some limitations.

Further, we also observed shortcomings in the model. The impact from BC has probably been underestimated, which affects the results for road transport but has very little effect for the other two sectors. We also observed a significant negative temperature response from aviation at high latitudes, probably caused by sulfate aerosols. It is unclear whether this impact is very realistic. We found values for the O₃ radiative forcing which were considerably smaller than those found in other studies for similar perturbations. Although the O₃ impact in the lower troposphere was well described using the extended linear ozone scheme, there were important differences in the upper troposphere and lower stratosphere for the impact from aviation.

The results presented here are obtained using only one AOGCM, and therefore the results should be interpreted with

care. Impacts on modeled temperature are closely related to the climate sensitivity of the model, and the climate sensitivity is known to vary significantly among models (IPCC, 2007, Table S8.1). However, relative impacts of the transport sectors w.r.t. the total anthropogenic climate impact are probably rather robust. The emissions that are the basis for this study are based on the SRES scenario A1B storyline for GDP development. This scenario is only one out of more GDP scenarios (Nakicenovic et al., 2000). Moreover alternative assumptions for the implementation of fuel efficiency and emission factors for the same A1B storyline have been suggested (Lee et al., 2009; Eyring et al., 2005).

The modeling of impacts from transport would benefit from the description of ice supersaturation in the model, and the possibility to advect tracers which might be beneficial for the contrail parametrization, the extended O₃ parametrization, or for the inclusion of small scale chemistry effects (Cariolle et al., 2009). In addition, a more extensive chemistry, an explicit description of aerosol processes, and an integrated carbon cycle would further increase the model's capability to describe impacts from transport. This would allow a more coherent modeling and limit the dependency on results from other models.

Although 2100 was the time horizon for our simulations based on the SRES scenario A1B, climate change is clearly not stabilized at that time: one can still see strong trends in the CO₂ forcings and in the response of the surface air temperature and ocean temperature. It is clear that in 2100 the CO₂ impacts (total anthropogenic impact and individual transport sectors) are still increasing considerably, suggesting further important changes in the 22nd century.

Acknowledgements. This work was supported by the European Union FP6 Integrated Project QUANTIFY (<http://www.ip-quantify.eu/>) under contract no. 003893 (GOCE). We would like to thank Marianne Lund for providing CO₂ mixing ratio time series, Gaby Rädcl for providing time series for CFC-12 and HFC-134a emission estimates, Pascal Laveau for his work on the extended linear O₃ scheme, and Keith Shine for useful discussions and his comments on the manuscript. We gratefully acknowledge the work of Activity 1 in the QUANTIFY project for creating emission estimates for the transport sector.

Edited by: M. Schulz



The publication of this article is financed by CNRS-INSU.

References

- Bakan, S., Betancor, M., Gayler, V., and Gral, H.: Contrail frequency over Europe from NOAA-satellite images, *Ann. Geophys.*, 12, 962–968, doi:10.1007/s00585-994-0962-y, 1994.
- Balkanski, Y., Myhre, G., Gauss, M., Rädcl, G., Highwood, E. J., and Shine, K. P.: Direct radiative effect of aerosols emitted by transport: from road, shipping and aviation, *Atmos. Chem. Phys.*, 10, 4477–4489, doi:10.5194/acp-10-4477-2010, 2010.
- Berntsen, T. and Fuglestedt, J.: Global temperature responses to current emissions from the transport sectors, *P. Natl. Acad. Sci. USA*, 105, 19154–19159, 2008.
- Borken, J., Steller, H., Merétei, T., and Vanhove, F.: Global and country inventory of road passenger and freight transportation: fuel consumption and emissions of air pollutants in year 2000, *Journal of the Transportation Research Board*, 2011, 127–136, doi:10.3141/2011-14, 2007.
- Boucher, O. and Lohmann, U.: The sulfate-CNN-cloud albedo effect: a sensitivity study with two general circulation models, *Tellus*, 47B, 281–300, 1995.
- Boucher, O. and Reddy, M. S.: Climate trade-off between black carbon and carbon dioxide emissions, *Energ. Policy*, 36, 193–200, doi:10.1016/j.enpol.2007.08.039, 2008.
- Boucher, O. and Rodhe, H.: The sulfate-CNN-cloud albedo effect: a sensitivity study, *Tech. Rep. 83*, Department of Meteorology, Stockholm University, Sweden, 1994.
- Bougeault, P.: A simple parameterization of the large-scale effects of cumulus, *Mon. Weather Rev.*, 113, 2108–2121, 1985.
- Brasseur, G. P., Müller, J.-F., and Granier, C.: Atmospheric impact of NO_x emissions by subsonic aircraft: A three-dimensional model study, *J. Geophys. Res.*, 101, 1423–1428, 1996.
- Brasseur, G. P., Cox, R. A., Hauglustaine, D., Isaksen, I., Lelieveld, J., Lister, D. H., Sausen, R., Schumann, U., Wahner, A., and Wiesen, P.: European scientific assessment of the atmospheric effects of aircraft emissions, *Atmos. Environ.*, 32, 2329–2418, 1998.
- Brasseur, G. P., Schultz, M., Granier, C., Saunio, M., Diehl, T., Botzet, M., Roeckner, E., and Walters, S.: Impact of climate change on the future chemical composition of the global troposphere, *J. Climate*, 19, 3932–3951, 2006.
- Brohan, P., Kennedy, J. J., Haris, I., Tett, S. F. B., and Jones, P. D.: Uncertainty estimates in regional and global observed temperature changes: a new dataset from 1850, *J. Geophys. Res.*, 111, D12106, doi:10.1029/2005JD006548, 2006.
- Burkhardt, U. and Kärcher, B.: Process-based simulation of contrail cirrus in a global climate model, *J. Geophys. Res.*, 114, D16201, doi:10.1029/2008JD011491, 2009.
- Burkhardt, U. and Kärcher, B.: Global radiative forcing from contrail cirrus, *Nature Climate Change*, 1, 54–58, doi:10.1038/NCLIMATE1086, 2011.
- Cariolle, D. and Déqué, M.: Southern hemisphere medium-scale waves and total ozone disturbances in a spectral general circulation model, *J. Geophys. Res.*, 91, 10825–10846, 1986.
- Cariolle, D. and Teyssède, H.: A revised linear ozone photochemistry parameterization for use in transport and general circulation models: multi-annual simulations, *Atmos. Chem. Phys.*, 7, 2183–2196, doi:10.5194/acp-7-2183-2007, 2007.
- Cariolle, D., Lasserre-Bigory, A., and Royer, J. F.: A general circulation model simulation of the springtime Antarctic ozone decrease and its impact on mid-latitudes, *J. Geophys. Res.*, 95, 1883–1898, 1990.
- Cariolle, D., Caro, D., Paoli, R., Hauglustaine, D. A., Cuénot, B., Cozic, A., and Paugam, R.: Parameterization of plume chemistry into large-scale atmospheric models: Application to aircraft NO_x emissions, *J. Geophys. Res.*, 114, D19302, doi:10.1029/2009JD011873, 2009.
- Champeaux, J. L., Masson, V., and Chauvin, F.: ECOCLIMAP: a global database of land surface parameters at 1 km resolution, *Meteorol. Appl.*, 12, 29–32, doi:10.1017/S1350482705001519, 2005.
- Clodic, D., Baker, J., Chen, J., Hirata, T., Hwang, R., Köhler, J., Petitjean, C., and Suwono, A.: IPCC/TEAP Special Report. Safeguarding the ozone layer and the global climate system: issues related to hydrofluorocarbons and perfluorocarbons, Cambridge University Press, Cambridge, United Kingdom and New York, NY, USA, 478 pp., 2005.
- Collins, W. J., Sitch, S., and Boucher, O.: How vegetation impacts affect climate metrics for ozone precursors, *J. Geophys. Res.*, 115, D23308, doi:10.1029/2010JD014187, 2010.
- Dahlmann, K., Grewe, V., Ponater, M., and Matthes, S.: Quantifying the contributions of individual NO_x sources to the trend in ozone radiative forcing, *Atmos. Environ.*, 45, 2860–2868, doi:10.1016/j.atmosenv.2011.02.071, 2011.
- Eide, M. S., Endresen, Ø., Mjelde, A., Mangset, L. E., and Gravir, G.: Ship emissions of the future, *Tech. Rep. 2007-1325*, Det

- Norske Veritas, Høvik, Norway, 2007.
- Endresen, O., Sorgard, E., Sundet, J. K., Dalsoren, S., Isaksen, I. S. A., Berglen, T., and Gravir, G.: Emission from international sea transportation and environmental impact, *J. Geophys. Res.*, 108, 4560, doi:10.1029/2002JD002898, 2003.
- Eyring, V., Köhler, H. W., Lauer, A., and Lemper, B.: Emissions from international shipping: 2. Impact of future technologies on scenarios until 2050, *J. Geophys. Res.*, 110, D17306, doi:10.1029/2004JD005620, 2005.
- Eyring, V., Stevenson, D. S., Lauer, A., Dentener, F. J., Butler, T., Collins, W. J., Ellingsen, K., Gauss, M., Hauglustaine, D. A., Isaksen, I. S. A., Lawrence, M. G., Richter, A., Rodriguez, J. M., Sanderson, M., Strahan, S. E., Sudo, K., Szopa, S., van Noije, T. P. C., and Wild, O.: Multi-model simulations of the impact of international shipping on Atmospheric Chemistry and Climate in 2000 and 2030, *Atmos. Chem. Phys.*, 7, 757–780, doi:10.5194/acp-7-757-2007, 2007.
- Eyring, V., Isaksen, I. S. A., Berntsen, T., Collins, W. J., Corbett, J. J., Endresen, O., Grainger, R. G., Moldanova, J., Schlager, H., and Stevenson, D. S.: Transport impacts on atmosphere and climate: Shipping, *Atmos. Environ.*, 44, 4735–4771, doi:10.1016/j.atmosenv.2009.04.059, 2010.
- Fuglestedt, J., Berntsen, T., Isaksen, I., Mao, H., Liang, X.-Z., and Wang, W.-C.: Climatic forcing of nitrogen oxides through changes in tropospheric ozone and methane; global 3D model studies, *Atmos. Environ.*, 33, 961–977, 1999.
- Fuglestedt, J., Berntsen, T., Myhre, G., Rypdal, K., and Skeie, R. B.: Climate forcing from the transport sectors, *P. Natl. Acad. Sci. USA*, 105, 454–458, 2008.
- Fuglestedt, J. S., Shine, K. P., Berntsen, T., Cook, J., Lee, D. S., Stenke, A., Skeie, R. B., Velders, G. J. M., and Waitz, I. A.: Transport impacts on atmosphere and climate: Metrics, *Atmos. Environ.*, 44, 4648–4677, doi:10.1016/j.atmosenv.2009.04.044, 2010.
- Gauss, M., Isaksen, I. S. A., Lee, D. S., and Søvde, O. A.: Impact of aircraft NO_x emissions on the atmosphere – trade-offs to reduce the impact, *Atmos. Chem. Phys.*, 6, 1529–1548, doi:10.5194/acp-6-1529-2006, 2006.
- Granier, C. and Brasseur, G. P.: The impact of road traffic on global tropospheric ozone, *Geophys. Res. Lett.*, 30, 1086, doi:10.1029/2002GL015972, 2003.
- Granier, C., Niemeier, U., Jungclaus, J. H., Emmons, L., Hess, P., Lamarque, J.-F., Walters, S., and Brasseur, G. P.: Ozone pollution from future ship traffic in the Arctic northern passages, *Geophys. Res. Lett.*, 33, L13807, doi:10.1029/2006GL026180, 2006.
- Gregory, J. M., Ingram, W. J., Palmer, M. A., Jones, G. S., Stott, P. A., Thorpe, R. B., Lowe, J. A., Johns, T. C., and Williams, K. D.: A new method for diagnosing radiative forcing and climate sensitivity, *Geophys. Res. Lett.*, 31, L03205, doi:10.1029/2003GL018747, 2004.
- Guémas, V. and Salas-Méla, D.: Simulation of the Atlantic meridional overturning circulation in an atmosphere-ocean global coupled model. Part I: a mechanism governing the variability of ocean convection in a preindustrial experiment, *Clim. Dynam.*, 31, 29–48, doi:10.1007/s00382-007-0336-8, 2008.
- Harvey, D., Gregory, J., Hoffert, M., Jain, A., Lal, M., Leemans, R., Raper, S., Wigley, T., and de Wolde, J.: An introduction to simple climate models used in the IPCC second assessment report, 1997.
- Hasselmann, K., Sausen, R., Maier-Reimer, E., and Voss, R.: On the cold start problem in transient simulations with coupled atmosphere-ocean models, *Clim. Dynam.*, 9, 53–61, 1993.
- Hedegaard, G. B., Brandt, J., Christensen, J. H., Frohn, L. M., Geels, C., Hansen, K. M., and Stendel, M.: Impacts of climate change on air pollution levels in the Northern Hemisphere with special focus on Europe and the Arctic, *Atmos. Chem. Phys.*, 8, 3337–3367, doi:10.5194/acp-8-3337-2008, 2008.
- Hodnebrog, Ø., Berntsen, T. K., Dessens, O., Gauss, M., Grewe, V., Isaksen, I. S. A., Koffi, B., Myhre, G., Olivie, D., Prather, M. J., Pyle, J. A., Stordal, F., Szopa, S., Tang, Q., van Velthoven, P., Williams, J. E., and Ødemark, K.: Future impact of non-land based traffic emissions on atmospheric ozone and OH – an optimistic scenario and a possible mitigation strategy, *Atmos. Chem. Phys.*, 11, 11293–11317, doi:10.5194/acp-11-11293-2011, 2011.
- Hoor, P., Borken-Kleefeld, J., Caro, D., Dessens, O., Endresen, O., Gauss, M., Grewe, V., Hauglustaine, D., Isaksen, I. S. A., Jöckel, P., Lelieveld, J., Myhre, G., Meijer, E., Olivie, D., Prather, M., Schnadt Poberaj, C., Shine, K. P., Staehelin, J., Tang, Q., van Aardenne, J., van Velthoven, P., and Sausen, R.: The impact of traffic emissions on atmospheric ozone and OH: results from QUANTIFY, *Atmos. Chem. Phys.*, 9, 3113–3136, doi:10.5194/acp-9-3113-2009, 2009.
- IPCC: Climate change 1995: the science of climate change. Contribution of working group I to the second assessment report of the intergovernmental panel on climate change, Cambridge University Press, Cambridge, United Kingdom and New York, NY, USA, 572 pp., 1996.
- IPCC: Climate change 2001: the scientific basis. Contribution of working group I to the third assessment report of the intergovernmental panel on climate change, Cambridge University Press, Cambridge, United Kingdom and New York, NY, USA, 881 pp., 2001.
- IPCC: Climate change 2007: the physical science basis. Contribution of working group I to the fourth assessment report of the intergovernmental panel on climate change, Cambridge University Press, Cambridge, United Kingdom and New York, NY, USA, 996 pp., 2007.
- Jiang, K., Masui, T., Morita, T., and Matsuoka, Y.: Long-term GHG emission scenarios for Asia-Pacific and the world, *Technol. Forecast. Soc.*, 63, 207–229, doi:10.1016/S0040-1625(99)00110-9, 2000.
- Johns, T. C., Royer, J.-F., Höschel, I., Huebener, H., Roeckner, E., Manzini, E., May, W., Dufresne, J.-L., Otterå, O. H., van Vuren, D. P., Salas y Melia, D., Giorgetta, M. A., Denvil, S., Yang, S., Fogli, P. G., Körper, J., Tjiputra, J. F., Stehfest, E., and Hewitt, C. D.: Climate change under aggressive mitigation: The ENSEMBLES multi-model experiment, *Clim. Dynam.*, 37, 1975–2003, doi:10.1007/s00382-011-1005-5, 2011.
- Joshi, M., Shine, K., Ponater, M., Stuber, N., Sausen, R., and Li, L.: A comparison of climate response to different radiative forcings in three general circulation models: towards an improved metric of climate change, *Clim. Dynam.*, 20, 843–854, 2003.
- Kärcher, B., Burkhardt, U., Ponater, M., and Frömming, C.: Importance of representing optical depth variability for estimates of global line-shaped contrail radiative forcing, *P. Natl. Acad. Sci. USA*, 107, 19181–19184, 2010.
- Kentarchos, A. S. and Roelofs, G. J.: Impact of aircraft NO_x emissions on tropospheric ozone calculated with a chemistry-general

- circulation model: Sensitivity to higher hydrocarbon chemistry, *J. Geophys. Res.*, 107, 4175, doi:10.1029/2001JD000828, 2002.
- Koffi, B., Szopa, S., Cozic, A., Hauglustaine, D., and van Velthoven, P.: Present and future impact of aircraft, road traffic and shipping emissions on global tropospheric ozone, *Atmos. Chem. Phys.*, 10, 11681–11705, doi:10.5194/acp-10-11681-2010, 2010.
- Lee, D. S., Fahey, D. W., Forster, P. M., Newton, P. J., Wit, R. C. N., Lim, L. L., Owen, B., and Sausen, R.: Aviation and global climate change in the 21st century, *Atmos. Environ.*, 43, 3520–3537, 2009.
- Lee, D. S., Pitari, G., Grewe, V., Gierens, K., Penner, J. E., Petzold, A., Prather, M. J., Schumann, U., Bais, A., Bernsten, T., Iachetti, D., Lim, L., and Sausen, R.: Transport impacts on atmosphere and climate: Aviation, *Atmos. Environ.*, 44, 4678–4734, doi:10.1016/j.atmosenv.2009.06.005, 2010.
- Lim, L., Lee, D. S., Sausen, R., and Ponater, M.: Quantifying the effects of aviation on radiative forcing and temperature with a climate response model, in: Proceedings of an international conference on transport, atmosphere and climate (TAC), edited by: Sausen, R., Blum, A., Lee, D. S., and Brüning, C., 202–207, <http://www.pa.op.dlr.de/tac/proceedings.html>, 2007.
- Liu, X., Penner, J. E., and Wang, M.: Influence of anthropogenic sulfate and black carbon on upper tropospheric clouds in the NCAR CAM3 model coupled to the IMPACT global aerosol model, *J. Geophys. Res.*, 113, D03204, doi:10.1029/2008JD010492, 2009.
- Mannstein, H., Meyer, R., and Wendling, P.: Operational detection of contrails from NOAA-AVHRR-data, *Int. J. Remote Sens.*, 20, 1641–1660, 1998.
- Marquart, S., Ponater, M., Mager, F., and Sausen, R.: Future development of contrail cover, optical depth, and radiative forcing: impacts of increasing air traffic and climate change, *J. Climate*, 16, 2890–2904, 2003.
- Matthes, S., Grewe, V., Sausen, R., and Roelofs, G.-J.: Global impact of road traffic emissions on tropospheric ozone, *Atmos. Chem. Phys.*, 7, 1707–1718, doi:10.5194/acp-7-1707-2007, 2007.
- Meinshausen, M., Raper, S., and Wigley, T.: Emulating coupled atmosphere-ocean and carbon cycle models with a simpler model, MAGICC6 – Part 1: Model description and calibration, *Atmos. Chem. Phys.*, 11, 1417–1456, doi:10.5194/acp-11-1417-2011, 2011a.
- Meinshausen, M., Wigley, T., and Raper, S.: Emulating atmosphere-ocean and carbon cycle models with a simpler model, MAGICC6 – Part 2: Applications, *Atmos. Chem. Phys.*, 11, 1457–1471, doi:10.5194/acp-11-1417-2011, 2011b.
- Millero, F. J. and Poisson, A.: International one-atmosphere equation of state of seawater, *Deep-Sea Res.*, 28A, 625–629, 1981.
- Minnis, P., Ayers, J. K., Palikonda, R., and Phan, D.: Contrails, cirrus trends, and climate, *J. Climate*, 17, 1671–1685, 2004.
- Morcrette, J.-J.: Impact of changes to the radiation transfer parameterizations plus cloud optical properties in the ECMWF model, *Mon. Weather Rev.*, 118, 847–873, 1990.
- Morcrette, J.-J.: Radiation and cloud radiative properties in the European Centre for Medium Range Weather Forecasts forecasting system, *J. Geophys. Res.*, 96, 9121–9132, doi:10.1029/89JD01597, 1991.
- Myhre, G., Kvalevåg, M., Rädcl, G., Cook, J., Shine, K. P., Clark, H., Karcher, F., Markowicz, K., Kardas, A., Wolkenberg, P., Balkanski, Y., Ponater, M., Forster, P., Rap, A., and de Leon, R. R.: Intercomparison of radiative forcing calculations of stratospheric water vapour and contrails, *Meteorol. Zeitschrift*, 18, 585–596, 2009.
- Myhre, G., Shine, K., Rädcl, G., Gauss, M., Isaksen, I., Tang, Q., Prather, M., Williams, J., van Velthoven, P., Dessens, O., Koffi, B., Szopa, S., Hoor, P., Grewe, V., Borken-Kleefeld, J., Bernsten, T., and Fuglested, J.: Radiative forcing due to changes in ozone and methane caused by the transport sector, *Atmos. Environ.*, 45, 387–394, doi:10.1016/j.atmosenv.2010.10.001, 2011.
- Nakicenovic, N., Alcamo, J., Davis, G., de Vries, B., Fenhann, J., Gaffin, S., Gregory, K., Grübler, A., Jung, T. Y., Kram, T., Rovere, E. L. L., Michaelis, L., Mori, S., Morita, T., Pepper, W., Pitcher, H., Price, L., Riahi, K., Roehrl, A., Rogner, H.-H., Sankovski, A., Schlesinger, M., Shukla, P., Smith, S., Swart, R., van Rooijen, S., Victor, N., and Dadi, Z.: Emissions scenarios, Cambridge University Press, Cambridge, United Kingdom and New York, NY, USA, 2000.
- Niemeier, U., Granier, C., Kornblueh, L., Walters, S., and Brasseur, G. P.: Global impact of road traffic on atmospheric chemical composition and on ozone climate forcing, *J. Geophys. Res.*, 111, D09301, doi:10.1029/2005JD006407, 2006.
- Oki, T. and Sud, Y. C.: Design of Total Runoff Integrating Pathways (TRIP) – A global river channel network, *Earth Interact.*, 2, 1–36, 1998.
- Oki, T., Wishimya, T., and Dirmeyer, P.: Assessment of annual runoff from land surface models using Total Runoff Integrating Pathways (TRIP), *J. Meteor. Soc. Japan*, 77, 235–255, 1999.
- Olivié, D. and Stuber, N.: Emulating AOGCM results using simple climate models, *Clim. Dynam.*, 35, 1257–1287, doi:10.1007/s00382-009-0725-2, 2010.
- Owen, B., Lee, D. S., and Lim, L.: Flying into the future: aviation emissions scenarios to 2050, *Environ. Sci. Technol.*, 44, 2255–2260, doi:10.1126/science.1196285, 2010.
- Paugam, R., Paoli, R., and Cariolle, D.: Influence of vortex dynamics and atmospheric turbulence on the early evolution of a contrail, *Atmos. Chem. Phys.*, 10, 3933–3952, doi:10.5194/acp-10-3933-2010, 2010.
- Penner, J. E., Lister, D. H., Griggs, D. J., Dokken, D. J., and McFarland, M. (Eds.): Aviation and the global atmosphere, Cambridge University Press, Cambridge, United Kingdom and New York, NY, USA, 1999.
- Penner, J. E., Chen, Y., Wang, M., and Liu, X.: Possible influence of anthropogenic aerosols on cirrus clouds and anthropogenic forcing, *Atmos. Chem. Phys.*, 9, 879–896, doi:10.5194/acp-9-879-2009, 2009.
- Ponater, M., Marquart, S., Sausen, R., and Schumann, U.: On contrail climate sensitivity, *Geophys. Res. Lett.*, 32, L10706, doi:10.1029/2005GL022580, 2005.
- Ponater, M., Pechtl, S., Sausen, R., Schumann, U., and Hüttig, G.: A state-of-the-art assessment of the potential of the cryoplane technology to reduce aircraft climate impact, *Atmos. Environ.*, 40, 6928–6944, 2006.
- Prather, M. J.: Lifetimes and eigenstates in atmospheric chemistry, *Geophys. Res. Lett.*, 21, 801–804, 1994.
- Quaas, J. and Boucher, O.: Constraining the first aerosol indirect radiative forcing in the LMDZ GCM using POLDER and MODIS satellite data, *Geophys. Res. Lett.*, 32, L17814,

- doi:10.1029/2005GL023850, 2005.
- Rädel, G. and Shine, K. P.: Radiative forcing by persistent contrails and its dependence on cruise altitudes, *J. Geophys. Res.*, 113, D07105, doi:10.1029/2007JD009117, 2008.
- Rap, A., Forster, P. M., Jones, A., Boucher, O., Bellouin, J. M. H. N., and Leon, R. R. D.: Parameterization of contrails in the UK Met Office Climate Model, *J. Geophys. Res.*, 115, D10205, doi:10.1029/2009JD012443, 2010.
- Ricard, J.-L. and Royer, J.-F.: A statistical cloud scheme for use in an AGCM, *Ann. Geophysicae*, 11, 1095–1115, 1993.
- Salas-Méllia, D.: A global coupled sea ice-ocean model, *Ocean Modelling*, 4, 137–172, 2002.
- Salas-Méllia, D., Chauvin, F., Déqué, M., Douville, H., Guérémy, J. F., Marquet, P., Planton, S., Royer, J., and Tyteca, S.: Description and validation of the CNRM-CM3 global coupled model, Tech. Rep. 103, CNRM, 2005.
- Sausen, R. and Schumann, U.: Estimates of the climate response to aircraft CO₂ and NO_x emissions scenarios, *Climate Change*, 44, 27–58, 2000.
- Sausen, R., Isaksen, I., Grewe, V., Hauglustaine, D., Lee, D. S., Myhre, G., Köhler, M. O., Pitari, G., Schumann, U., Stordal, F., and Zerefos, C.: Aviation radiative forcing in 2000: an update on IPCC (1999), *Meteorol. Zeitschrift*, 14, 555–561, 2005.
- Schumann, U.: On conditions for contrail formation from aircraft exhausts, *Meteorol. Zeitschrift*, 5, 4–23, 1996.
- Sitch, S., Cox, P. M., Collins, W. J., and Huntingford, C.: Indirect radiative forcing of climate change through ozone effects on the land-carbon sink, *Nature*, 448, 791–794, doi:10.1038/nature06059, 2007.
- Skeie, R. B., Fuglestedt, J., Berntsen, T., Lund, M. T., Myhre, G., and Rypdal, K.: Global temperature change from the transport sectors: Historical development and future scenarios, *Atmos. Environ.*, 43, 6260–6270, 2009.
- Stevenson, D. S., Doherty, R. M., Sanderson, M. G., Collins, W. J., Johnson, C. E., and Derwent, R. G.: Radiative forcing from aircraft NO_x emissions: Mechanisms and seasonal dependence, *J. Geophys. Res.*, 109, D17307, doi:10.1029/2004JD004759, 2004.
- Stordal, F., Myhre, G., Stordal, E. J. G., Rossow, W. B., Lee, D. S., Arlander, D. W., and Svendby, T.: Is there a trend in cirrus cloud cover due to aircraft traffic?, *Atmos. Chem. Phys.*, 5, 2155–2162, doi:10.5194/acp-5-2155-2005, 2005.
- Stuber, N., Sausen, R., and Ponater, M.: Stratosphere adjusted radiative forcing calculations in a comprehensive climate model, *Theor. Appl. Climatol.*, 68, 125–135, 2001.
- Stuber, N., Ponater, M., and Sausen, R.: Why radiative forcing might fail as a predictor of climate change, *Clim. Dynam.*, 24, 497–510, 2005.
- Teyssèdre, H., Michou, M., Clark, H. L., Josse, B., Karcher, F., Olivié, D., Peuch, V.-H., Saint-Martin, D., Cariolle, D., Attié, J.-L., Nédélec, P., Ricaud, P., Thouret, V., van der A, R. J., Volz-Thomas, A., and Chéroux, F.: A new tropospheric and stratospheric Chemistry and Transport Model MOCAGE-Climat for multi-year studies: evaluation of the present-day climatology and sensitivity to surface processes, *Atmos. Chem. Phys.*, 7, 5815–5860, doi:10.5194/acp-7-5815-2007, 2007.
- Trenberth, K. E.: The definition of El Niño, *B. Am. Meteorol. Soc.*, 78, 2771–2777, 1997.
- Uherek, E., Halenka, T., Borken-Kleefeld, J., Balkanski, Y., Berntsen, T., Borrego, C., Gauss, M., Hoor, P., Juda-Rezler, K., Lelieveld, J., Melas, D., Rypdal, K., and Schmid, S.: Transport impacts on atmosphere and climate: land transport, *Atmos. Environ.*, 44, 4772–4816, doi:10.1016/j.atmosenv.2010.01.002, 2010.
- Watterson, I. G.: Non-dimensional measures of climate performance, *Int. J. Climatol.*, 16, 379–391, 1996.
- WMO: Scientific assessment of ozone depletion: 2010, no. 52 in Global ozone research and monitoring project report, Geneva, 2010.
- Wu, S., Mickley, L. J., Jacob, D. J., Rind, D., and Streets, D. G.: Effects of 2000–2050 changes in climate and emissions on global tropospheric ozone and the policy-relevant background surface ozone in the United States, *J. Geophys. Res.*, 113, D18312, doi:10.1029/2007JD009639, 2008.